



Hydrodynamics of a flexible cylinder under modulated vortex-induced vibrations

Chang Liu ^{a,b,c}, Shixiao Fu ^{a,b,*}, Mengmeng Zhang ^{a,b,*}, Haojie Ren ^{a,b},
Yuwang Xu ^{a,b}

^a State Key Laboratory of Ocean Engineering, Shanghai Jiao Tong University, Shanghai 200240, China

^b Collaborative Innovation Centre for Advanced Ship and Deep-Sea Exploration, Shanghai 200240, China

^c Department of Mechanical Engineering, Johns Hopkins University, Baltimore, MD 21218, USA



ARTICLE INFO

Article history:

Received 9 April 2019

Received in revised form 3 November 2019

Accepted 6 February 2020

Available online xxxx

Keywords:

Modulated vortex-induced vibration

Time-varying hydrodynamics

Forgetting Factor Least Squares method

Amplitude modulation

Frequency modulation

ABSTRACT

Both amplitude modulation and frequency modulation of Vortex-induced Vibration (VIV) are observed in a recent model test of a flexible cylinder under oscillatory flow, but its hydrodynamics has not yet been broached in detail. This paper employs the Forgetting Factor Least Squares (FF-LS) method for identification of time-varying hydrodynamics of a flexible cylinder under modulated VIV. The FF-LS method's applicability to accurately identify time-varying hydrodynamic coefficients is demonstrated through an elastically mounted rigid cylinder under flow with a given modulated motion. Furthermore, we propose a framework to predict instantaneous amplitude (envelope) and frequency using time-varying hydrodynamic coefficients to establish their analytical relationship. This prediction method is further extended to a highly tensioned flexible cylinder through Fourier series expansion in the spatial domain. By performing the identification procedure for all sampled data of a flexible cylinder undergoing oscillatory flow, we obtain the corresponding time-varying hydrodynamics in the cross-flow direction considering the amplitude and frequency modulation. The results show that, under modulated VIV, hydrodynamic coefficients of the flexible cylinder also show time-varying characteristics. We further investigate differences between identified hydrodynamic coefficients and those obtained from the database of a cylinder with modulated motion under flow. Prediction results using these identified time-varying coefficients reveal that the time-varying excitation coefficients mainly influence the amplitude modulation, and the time-varying added-mass coefficients contain the major information of frequency modulation. These results further suggest including the temporal derivative of the instantaneous amplitude as one determining parameter in building databases to improve the prediction of modulated VIV.

© 2020 Elsevier Ltd. All rights reserved.

1. Introduction

The commonly used semi-empirical programs to predict Vortex-induced Vibration (VIV) damage for slender marine structures are SHEAR7 (Vandiver and Li, 2005), VIVA (Triantafyllou, 2003), and VIVANA (Larsen et al., 2001). See reviews in Chaplin et al. (2005a) and Wu et al. (2012). These tools use semi-empirical models relying on hydrodynamic force

* Corresponding authors at: State Key Laboratory of Ocean Engineering, Shanghai Jiao Tong University, Shanghai 200240, China.
E-mail addresses: shixiao.fu@sjtu.edu.cn (S. Fu), claire_zhang@sjtu.edu.cn (M. Zhang).

coefficients identified in VIV model tests. Thus, the accuracy of these coefficients used in the construction of vortex-induced force directly determines the accuracy of VIV prediction results. The present existing hydrodynamic force coefficient database used in the semi-empirical prediction models for VIV is obtained from a one-degree-of-freedom forced oscillation test of a rigid cylinder in a pure Cross-Flow (CF) direction (Gopalkrishnan, 1993) or in a pure In-Line (IL) direction (Aronsen, 2007; Aronen and Larsen, 2007).

However, in real conditions, the VIV of a flexible cylinder exists in both CF and IL directions, and the vibrations in these two directions are strongly coupled (Song et al., 2017; Wu et al., 2016). This kinematic coupling leads to an interaction of the hydrodynamic forces in these two directions (Jauvtis and Williamson, 2003, 2004; Dahl et al., 2007). Furthermore, different excited vibration modes of flexible cylinders also interacted with the surrounding flow field. These make the hydrodynamics of flexible cylinders different from the results obtained from the forced oscillation test of the rigid cylinder in a single direction (Sumer, 2006; Marollo and Hinwood, 2006).

In order to discern the hydrodynamics of flexible cylinders under VIV, the Euler-Bernoulli beam equation is employed to obtain the vortex-induced force of a flexible cylinder under multi-mode vortex-induced vibrations (Chaplin et al., 2005b; Huera-Huarte et al., 2006; Huera-Huarte and Bearman, 2009a,b). Focusing on the lock-in frequency, Song et al. (2016a,b) used the method of modal analysis combined with the Euler beam dynamic response equation to analyze hydrodynamic force and its coefficients. Results revealed that the obtained hydrodynamic coefficients of flexible cylinders under VIV were different from those of the rigid cylinder.

The aforementioned research focused on the hydrodynamics of VIV under single steady response frequency; i.e., the lock-in frequency of VIV. However, an intermittent VIV was found occasionally in the sag bend close to the Touchdown Point (TDP) of a Steel Catenary Riser (SCR) from the Joint Industrial Program called STRIDE (Grant et al., 1999) carried out in the United States. It was later demonstrated that this sort of VIV is excited not by steady flow, but by oscillatory flow relative to the riser due to heave motion of the vessel connected to the riser (Gonzalez, 2001). The dynamic response feature of this heave-induced VIV was investigated through finite element simulation (Chen et al., 2014), and the heave-induced VIV was also included in VIV prediction (Maher and Finn, 2000; Chang and Isherwood, 2003; Wu et al., 2015).

To confirm quantitatively that VIV occurs in oscillatory flow, Fu et al. (2013, 2014) conducted a model test of a flexible cylinder under relative oscillatory flow using a large-scale forced-oscillation device. The results exhibit that the vortex-induced vibrations show both amplitude modulation and time-varying vibration frequency; i.e., frequency modulation. Further model tests revealed that, under the vessel motion-induced oscillatory current, the out-of-plane VIV also exhibits amplitude modulation and frequency modulation features for both the free-hanging riser (Wang et al., 2016, 2017) and the steel catenary riser (Wang et al., 2015b, 2018).

The modulation phenomenon of VIV also exists for a flexible cylinder under uniform and shear flows. Brika and Laneville (1993) conducted a free vibration test of a flexible riser under uniform airflow and found the amplitude modulation (beating) phenomenon. In sheared and uniform ocean currents, Swithenbank (2007) found that the VIV response frequency of a flexible riser model test switches among different frequencies at different times, which also represents one type of frequency modulation. Bourguet et al. (2011, 2013) also observed a similar amplitude and frequency modulation through the simulation of a long flexible riser under shear flows. Furthermore, Evangelinos and Karniadakis (1999) observed that the traveling wave of a flexible riser under the turbulent state is subject to significant modulation compared with the laminar case from numerical simulation.

The modulated VIV also results from the axial top-motion excitation of the flexible riser; see e.g., da Silveira et al. (2009) and Franzini et al. (2009, 2010, 2015a,b, 2018). The variation of tension leads to the modulation of natural frequency, and a special experimental device (Franzini et al., 2009) was employed to study the effect of this natural frequency modulation on the response (da Silveira et al., 2009; Franzini et al., 2010, 2015a,b, 2018). Using Hilbert-Huang spectral analysis, these authors observed both amplitude and frequency modulation as well as parametric instability under certain top-motion tension frequency, which was found to significantly affect the response of a flexible cylinder. Aside from tension variation, the intrinsic nonlinear dynamics of the riser will also lead to the broad bandwidth frequency response, indicating that amplitude and frequency modulations exist. For example, dynamical response considering mid-plane stretching nonlinearity show internal resonances and chaotic behavior under harmonic or multifrequency external load (Alfossal and Younis, 2019a,b).

Modulated vortex-induced vibration also has a strong influence on fatigue damage for the flexible cylinder (Wang et al., 2015a), and thus the modulation effect of VIV cannot be neglected in the flexible riser design. Although response strain and displacement for out-of-plane VIV under the vessel motion-induced oscillatory current are smaller than those under uniform current, the damage caused by the vessel motion-induced VIV is comparable and at the same damage level as those under uniform current for both the steel catenary riser (Wang et al., 2014, 2018) and the free hanging riser (Wang et al., 2016, 2017). The increase of fatigue damage possibly results from the modulation effect of VIV (Swithenbank, 2007; Swithenbank and Vandiver, 2007), especially from underlying high frequency components.

To investigate the hydrodynamics of the modulated VIV, Gopalkrishnan (1993) conducted forced oscillation tests for a submerged rigid cylinder under modulated motion and obtained the database for hydrodynamic coefficients under 1:3, 1:10, and 1:20 modulation rates. When a cylinder displacement undergoes significant amplitude modulation, Hover et al. (1997, 1998) found that the force spectra are generally broadband in the lock-in regime. However, the hydrodynamic characteristics of a flexible cylinder under VIV with the amplitude and frequency modulations are not broached in detail in the afore-mentioned papers in that no effective analysis methods were developed.

This paper employs the Forgetting Factor Least Squares (FF-LS) method for identification of time-varying hydrodynamics of a flexible cylinder under modulated vortex-induced vibrations. Different from the method utilized by former researchers for identification of hydrodynamics (Song et al., 2016a), where equal weights were applied to all sampled data, this method introduces a forgetting factor to apply a greater weight on the data closer to the present moment. This forgetting factor plays the same role as the weighting factor in a closely related method employed to obtain a reduced order model for time-varying systems; i.e., online Dynamic Mode Decomposition (DMD) (Zhang et al., 2019). This method affords the possibility to identify the time-varying hydrodynamics. Section 2.1 describes the framework of time-varying hydrodynamics identification, and Section 2.2 illustrates this method on a modulated signal with known instantaneous amplitude and frequency.

The identified hydrodynamic coefficients offer a linear, yet time-varying, system to describe the vortex-induced vibration of a flexible cylinder under oscillatory flow. Recently developed online DMD (Zhang et al., 2019) and Sparse Identification of Nonlinear Dynamics (SINDy) (Brunton et al., 2016) offer further possibilities to identify the nonlinear time-varying model; see e.g., aerodynamics of a prototype bridge under VIV (Li et al., 2019). Nevertheless, in this paper, we restrict the system parameters needed to be estimated as time-varying excitation and added-mass coefficients and restrict our vortex-induced force as a linear combination of velocity and acceleration weighted with these time-varying coefficients. This restriction affords the physical interpretation of resulting time-varying hydrodynamic coefficients and allows us to reveal the hydrodynamic mechanism behind the modulated VIV.

To explore this mechanism, we developed a framework to predict instantaneous amplitude and frequency using previously obtained time-varying hydrodynamic coefficients. This framework is initially illustrated through an elastically mounted cylinder under flow (Section 3.1). Then the analytical relationship between the time-varying hydrodynamics and modulated VIV are established in Section 3.2. Finally, this framework is extended to the modulation prediction of a highly tensioned flexible cylinder (Section 3.3).

In Section 4, we apply the current identification and prediction frameworks to experimental data of a flexible cylinder (Section 4.1), where the VIV response is obtained through modal analysis, and vortex-induced force is obtained through the inverse analysis method (Section 4.2). Results of obtained time-varying vortex-induced force coefficients are shown in Section 4.3, and the influence of time-varying hydrodynamics on modulated VIV are analyzed in Section 4.4.

2. Time-varying hydrodynamics identification

2.1. Identification approach

Typically, hydrodynamics of a flexible cylinder under vortex-induced vibration is focused on lock-in frequency, which assumes that VIV is a steady simple harmonic vibration (Gopalkrishnan, 1993; Song et al., 2016a). Considering this assumption, VIV displacement in the CF direction is expressed as:

$$y(z, t) = y_0(z)\sin(\omega t + \phi_0). \quad (2.1)$$

In this equation, z is a spatial coordinate, which indicates a different axial position along the cylinder; t is the temporal coordinate, which means different moment. ω is vibration frequency; and ϕ_0 is the initial phase angle, both of which are constant. $y_0(z)$ is VIV displacement amplitude, which only changes over the axial position of the cylinder. $y(z, t)$ represents the time history of VIV displacement in the CF direction at the position z .

The VIV velocity and acceleration can be obtained through temporal differentiating Eq. (2.1):

$$\dot{y}(z, t) = y_0(z)\omega \cos(\omega t + \phi_0), \quad (2.2a)$$

$$\ddot{y}(z, t) = -y_0(z)\omega^2 \sin(\omega t + \phi_0). \quad (2.2b)$$

When VIV reaches the lock-in stage, the frequency of vortex-induced force, namely the frequency of vortex shedding, is assumed as VIV response frequency. The phase angle between hydrodynamic force and displacement is assumed as a constant under the lock-in stage (Zdravkovich, 1996), and, thus, vortex-induced force under this stage can be written as:

$$f_{CF}(z, t) = f_0(t)\sin(\omega t + \phi_0 + \theta_0), \quad (2.3)$$

where $f_0(z, t)$ is the force amplitude, and θ_0 is the phase angle between the hydrodynamic force and displacement at vibration frequency ω . Expanding the right hand side of Eq. (2.3) yields:

$$f_{CF}(z, t) = f_0(z)\sin(\theta_0)\cos(\omega t + \phi_0) - [-f_0(z)\cos(\theta_0)\sin(\omega t + \phi_0)]. \quad (2.4)$$

In the above equation, hydrodynamic force is divided into two parts: one is the excitation force, $f_e = f_0(z)\sin(\theta_0)\cos(\omega t + \phi_0)$, in phase with velocity $\dot{y}(z, t)$, and the other is the inertial component related to the added-mass concept, $f_a = -f_0(z)\cos(\theta_0)\sin(\omega t + \phi_0)$, in phase with acceleration $\ddot{y}(z, t)$.

Afterwards, these force parts are normalized into the excitation coefficient and the added-mass coefficient using the equation below, which is convenient for an engineering application:

$$f_0(z)\sin(\theta_0)\cos(\omega t + \phi_0) = \frac{\rho D l U^2(z, t)}{2v_0(z)} CLe(z)\dot{y}(z, t), \quad (2.5a)$$

$$-f_0(z)\cos(\theta_0)\sin(\omega t + \phi_0) = \frac{\rho\pi D^2 l}{4} CLa(z)\ddot{y}(z, t). \quad (2.5b)$$

In the above equation, $CLe(z)$ is called the excitation coefficient and $CLa(z)$ is called the added-mass coefficient. l is the element unit length; ρ is the fluid density; $U(z, t)$ is flow velocity relative to the center line of the cylinder at a cross section location z and instant t , and D is the hydrodynamic diameter of the cylinder. $v_0(z)$ is the amplitude of VIV velocity, which is equal to $\omega y_0(z)$ for single frequency motion.

Substituting Eqs. (2.5a) and (2.5b) into Eq. (2.4), hydrodynamic force is divided as:

$$f_{CF}(z, t) = \frac{\rho D l U^2(z, t)}{2v_0(z)} CLe(z)\dot{y}(z, t) - \frac{\rho\pi D^2 l}{4} CLa(z)\ddot{y}(z, t). \quad (2.6)$$

In the above equation, the hydrodynamic coefficient definition is the same as Song et al. (2016a) and Gopalkrishnan (1993). In solving hydrodynamic coefficients in this equation, we are attempting to find the excitation coefficient $CLe(z)$ and added-mass coefficient $CLa(z)$, which renders the right hand side of the equation equal the left.

When the flexible cylinder undergoes oscillatory motion, both amplitude modulation and frequency modulation (Swithenbank, 2007; Swithenbank and Vandiver, 2007; Fu et al., 2014; Wang et al., 2015b, 2016, 2017, 2018) are usually observed in vortex-induced vibration. Time-invariant hydrodynamic coefficients, which average varying information in the time domain, cannot consider the amplitude or frequency modulation effect of vortex-induced vibration.

This paper changes time-invariant hydrodynamic coefficients into time-varying coefficients as we attempt to capture the amplitude and frequency modulation effects in vortex-induced vibration. The time-varying hydrodynamic coefficient problem is defined as:

$$f_{CF}(z, t) = \frac{\rho D l U_{RMS}^2(z)}{2v_0(z)} CLe(z, t)\dot{y}(z, t) - \frac{\rho\pi D^2 l}{4} CLa(z, t)\ddot{y}(z, t). \quad (2.7)$$

In the above equation, the RMS (Root Mean Square) value of flow velocity, $U_{RMS}(z) = \sqrt{\frac{1}{T} \int_0^T U^2(z, t) dt}$, is chosen for normalization of the excitation coefficient to avoid the infinite value when normalizing excitation coefficients. For single frequency time-varying oscillatory flow, $\sqrt{2}U_{RMS}(z)$ is equal to the amplitude of flow velocity $U_0(z)$. When amplitude modulation occurs in VIV, velocity amplitude may also vary over time. $v_0(z)$ is chosen as the largest amplitude of VIV velocity for simplicity of further analysis. Choosing another variable of slow time scale and using multi-scale method (Bender and Orszag, 2013; Ilyas et al., 2019; Alfossail and Younis, 2019a,b; Champion et al., 2019) may provide further insight, but we reserve it for future work.

In Eq. (2.7), $CLe(z, t)$ and $CLa(z, t)$ are time-varying excitation coefficients and added-mass coefficients. We will demonstrate in the following section that the time-varying vortex-induced force coefficients, $CLe(z, t)$, $CLa(z, t)$, are able to take into account the amplitude and frequency modulation effect of VIV.

In particular, when the VIV response and force contain only one single frequency component, the obtained coefficient, $CLe(z, t)$, $CLa(z, t)$, will not change over time (Liu et al., 2017), and the definition of hydrodynamic coefficients is consistent with the hydrodynamic coefficients defined by Song et al. (2016a) and Gopalkrishnan (1993).

Then, we employ the *Forgetting Factor Least Squares* (FF-LS) method (Liu et al., 2018; Ding and Chen, 2005; Paleologu et al., 2008) to identify the time-varying vortex-induced force coefficients in Eq. (2.7). This method introduces a forgetting factor, which divides the time history of the sampling data into different regions and offers a greater weight to the data closer to the present moment. This modification improves the sensitivity of the Least Squares method and makes it possible to identify the time-varying parameters considering the amplitude and frequency modulation effects of VIV. For the time-varying hydrodynamics identification problem in Eq. (2.7), the time history of force, the response and time-varying coefficients at moment t_L can be individually expressed using matrices $\mathbf{f}_L \in \mathbb{R}^{L \times 1}$, $\mathbf{H}_L \in \mathbb{R}^{L \times 2}$, and $\boldsymbol{\theta}(L) \in \mathbb{R}^{2 \times 1}$:

$$\mathbf{f}_L := [f_{CF}(z, t_1) \ f_{CF}(z, t_2) \ f_{CF}(z, t_3) \ \cdots \ f_{CF}(z, t_L)]^T, \quad (2.8a)$$

$$\mathbf{H}_L := [\mathbf{h}(1) \ \mathbf{h}(2) \ \mathbf{h}(3) \ \cdots \ \mathbf{h}(L)]^T \quad (2.8b)$$

$$= \begin{bmatrix} \dot{y}(z, t_1) & \dot{y}(z, t_2) & \dot{y}(z, t_3) & \cdots & \dot{y}(z, t_L) \\ \ddot{y}(z, t_1) & \ddot{y}(z, t_2) & \ddot{y}(z, t_3) & \cdots & \ddot{y}(z, t_L) \end{bmatrix}^T, \text{ and} \quad (2.8c)$$

$$\boldsymbol{\theta}(L) := \begin{bmatrix} \frac{\rho D l U_{RMS}^2(z)}{2v_0(z)} CLe(z, t_L) \\ -\frac{\rho\pi D^2 l}{4} CLa(z, t_L) \end{bmatrix}, \ L = 1, 2, 3, \dots, \quad (2.8d)$$

where the superscript T indicates the transpose.

In the equation above, $t_1, t_2, t_3, \dots, t_L$ represent the sampling time, and L groups of data are sampled in total. z represents the spatial position of the data, and the rows of the above three matrices represent the values at different sampling instants of time. \mathbf{f}_L is the time history of vortex-induced force at node z from the initial moment t_1 to the present moment t_L . \mathbf{H}_L is the time history of velocity and acceleration at node z from the initial moment t_1 to the present

moment t_L . $\theta(L)$ is the dimensional vortex-induced force coefficient at node z at moment t_L . Identification of time-varying hydrodynamics can be written as identifying a set of time-varying parameters, $\theta(L)$, $L = 1, 2, 3, \dots$, which satisfy:

$$\mathbf{f}_L = \mathbf{H}_L \theta(L), \quad L = 1, 2, 3, \dots \quad (2.9)$$

Eq. (2.9) utilizes all previous historical moment data before t_L to identify time-varying parameters $\theta(L)$. Then, the sampled force and response at different moments are multiplied by different data weights. The data weight is bigger if the data is closer to the present moment t_L . Specifically, the data weight for the present moment is $\beta^0 = 1$, and the data weight for the initial moment is β^{L-1} (β is a constant, which satisfies $0 < \beta \leq 1$). The force and response with data weight multiplied are denoted as $\hat{\mathbf{f}}_L \in \mathbb{R}^{L \times 1}$ and $\hat{\mathbf{H}}_L \in \mathbb{R}^{L \times 2}$:

$$\hat{\mathbf{f}}_L := [\beta^{L-1} f_{CF}(z, t_1) \quad \beta^{L-2} f_{CF}(z, t_2) \quad \cdots \quad \beta f_{CF}(z, t_{L-1}) \quad f_{CF}(z, t_L)]^T, \quad (2.10a)$$

$$\hat{\mathbf{H}}_L := [\beta^{L-1} \mathbf{h}(1) \quad \beta^{L-2} \mathbf{h}(2) \quad \cdots \quad \beta \mathbf{h}(L-1) \quad \mathbf{h}(L)]^T. \quad (2.10b)$$

In this way, the solution model is rewritten as follows:

$$\hat{\mathbf{f}}_L = \hat{\mathbf{H}}_L \theta(L). \quad (2.11)$$

According to the basic principle of the Least Squares method (Chavent, 1979), the parameters to be identified need to minimize the sum of squared errors between $\hat{\mathbf{f}}_L$ and $\hat{\mathbf{H}}_L \theta(L)$; i.e.,

$$\min[(\hat{\mathbf{f}}_L - \hat{\mathbf{H}}_L \theta(L))^T (\hat{\mathbf{f}}_L - \hat{\mathbf{H}}_L \theta(L))]. \quad (2.12)$$

We have the solution for the least squares problem as:

$$\hat{\theta}(L) = (\hat{\mathbf{H}}_L^T \hat{\mathbf{H}}_L)^{-1} \hat{\mathbf{H}}_L^T \hat{\mathbf{f}}_L, \quad (2.13)$$

if $\hat{\mathbf{H}}_L^T \hat{\mathbf{H}}_L$ is not singular. Substituting Eqs. (2.10a) and (2.10b) into Eq. (2.13), we get the estimation of time-varying coefficients at the moment t_L :

$$\hat{\theta}(L) = \left[\sum_{i=1}^L \beta^{2(L-i)} \mathbf{h}(i) \mathbf{h}^T(i) \right]^{-1} \left[\sum_{i=1}^L \beta^{2(L-i)} \mathbf{h}(i) f_{CF}(z, t_i) \right] \quad (2.14a)$$

$$= \left[\sum_{i=1}^L \mu^{(L-i)} \mathbf{h}(i) \mathbf{h}^T(i) \right]^{-1} \left[\sum_{i=1}^L \mu^{(L-i)} \mathbf{h}(i) f_{CF}(z, t_i) \right] \quad (2.14b)$$

$$= (\mathbf{H}_L^T \Lambda_L \mathbf{H}_L)^{-1} \mathbf{H}_L^T \Lambda_L \mathbf{f}_L, \quad L = 1, 2, 3, \dots, \quad (2.14c)$$

where $\mu = \beta^2$, $0 < \mu \leq 1$; μ is called the *Forgetting Factor*. Λ_L is the weighted matrix, whose diagonal entries are $\Lambda(L) = 1$ and $\Lambda(k-1) = \mu \Lambda(k)$, and whose off-diagonal entries are 0.

The essence of this method is to assign different weights to the data. A smaller weight is put on the data that is farther away from the present moment as shown in Fig. 1. When setting the forgetting factor $\mu = 1$, this method is equivalent to the least squares method, where equal weights are assigned to all sampled data. Different from the band-pass filter employing a finite window in the frequency domain, the effect of this forgetting factor is similar to setting a finite window in the time domain. Data far away from the current instant are associated with negligible weights (≈ 0), and they can be viewed as outside of this finite window. As a result, this method is closely related to the moving least squares or local regression (Cleveland and Devlin, 1988; Levin, 1998). In addition, this idea of setting a finite window can be used to extend the spectral analysis using short-time Fourier analysis (Allen, 1977). This analysis has been applied to the hydrodynamic coefficients of a flexible cylinder at a high Reynolds number (Ren et al., 2018). Different from these methods with a finite window where a hard cutoff is employed, the forgetting factor in this FF-LS provides a soft cutoff on older data, and all of these approaches are effective in capturing the time-varying dynamics (Zhang et al., 2019).

To save memory and to speed up the algorithm for hydrodynamics identification, the FF-LS method proposed here can be rewritten as a recursive version; see Appendix A. Verification of this method for identifying time-varying parameters from a modulated signal is presented in the following subsections.

2.2. Illustration of identification method for a modulated motion

In this subsection, we illustrate the identification method for a synthesized modulated motion where we have the information of amplitude and frequency modulation *a priori*, which offers convenience for evaluating the performance of the following prediction method as well as building the analytical relationship between time-varying hydrodynamic coefficients and modulated motion. This synthesized signal is used to describe an elastically mounted rigid cylinder under flow (Govardhan and Williamson, 2000) with parameters in Table 1 to normalize identified results. The elastically mounted rigid cylinder under flow can be modeled as a forced mass-spring-dashpot system:

$$m\ddot{y}(t) + c\dot{y}(t) + ky(t) = F_{hydro}(t), \quad (2.15)$$

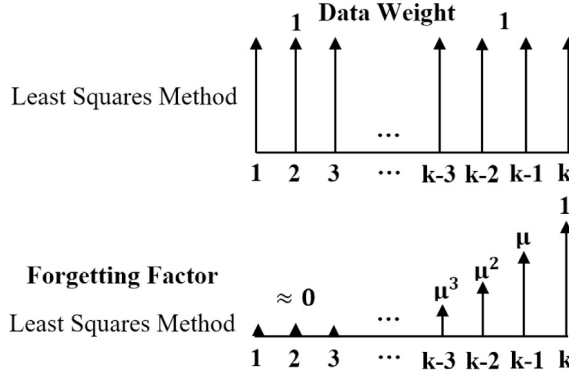


Fig. 1. The schematic of data weight for the Forgetting Factor Least Squares (FF-LS) method.

Table 1

The parameters of an elastically mounted rigid cylinder under uniform flow (Govardhan and Williamson, 2000).

Parameters	Value	Parameters	Value
Mass of cylinder m (kg)	3.7486	Mass ratio $m^* = \frac{m}{\pi \rho D^2 l/4}$	8.63
Damping c (kg/s)	0.07132	Natural frequency $f_N = \frac{1}{2\pi} \sqrt{\frac{k}{m}} (1 - \xi^2)$ (Hz)	1
Stiffness k (N/m)	147.989	Damping ratio $\xi = \frac{c}{2\sqrt{mk}}$	0.15%
Flow velocity U (m/s)	0.2667	Reduced velocity $U^* = \frac{U}{f_N D}$	7
Flow density ρ (kg/m ³)	1000	Length ratio l/D	20
Diameter of cylinder D (m)	0.0381	Amplitude ratio $A^* = A_{\max}/D$	0.6

Table 2

The parameters of the synthesized modulated signal in Eq. (2.16).

Parameters	Value	Parameters	Value
A_c (m)	0.02286	f_c (Hz)	1
A_{am} (m)	$0.85 \times A_c$	f_{am} (Hz)	0.1
A_{fm} (Hz)	$0.15 \times f_c$	f_{fm} (Hz)	0.2

where $F_{hydro}(t)$ is the hydrodynamic force acting on the cylinder and m , c , k are mass, damping of the dashpot and stiffness of the spring, respectively. We set these parameters as documented in Table 1, and they are kept as constants. Aware of the displacement signal $y(t)$, we can compute the velocity $\dot{y}(t)$ and acceleration $\ddot{y}(t)$ through temporal differentiating once and twice, respectively. According to the dynamics in Eq. (2.15), the hydrodynamic force signal $F_{hydro}(t)$ (added-mass force included) that causes this motion is obtained (Williamson and Govardhan, 2004).

For single frequency signal, the identified coefficients will not vary over time, and the FF-LS method yields the same results as the analytical solution (Liu et al., 2017). In this paper, we focus on the modulated signal:

$$y(t) = [A_c + m(t)] \sin(2\pi \int_0^t [f_c + f_m(\tau)] d\tau), \quad (2.16)$$

where $m(t) = A_{am} \cos(2\pi f_{am} t)$ represents amplitude modulation and $f_m(t) = A_{fm} \cos(2\pi f_{fm} t)$ represents frequency modulation, respectively. Here, we assume $0 \leq A_{am} \leq A_c$ and $0 \leq A_{fm} \leq f_c$. If $m(t) \equiv 0$, $\forall t$ and $f_m(\tau) \equiv 0$, $\forall \tau$, we can see that the motion signal in Eq. (2.16) becomes the sinusoidal; i.e., $y(t) = A_c \sin(2\pi f_c t)$, where both the amplitude A_c and frequency f_c are constant. In Eq. (2.16):

$$A_c + m(t) =: A_{tot}(t) \text{ and} \quad (2.17a)$$

$$f_c + f_m(t) =: f_{tot}(t) \quad (2.17b)$$

represent the instantaneous amplitude (envelope of the motion signal) and instantaneous frequency (Boashash, 2016), respectively. Here, the instantaneous frequency represents the change rate of the phase with respect to time. Fig. 2 depicts the time history and Power Spectral Density (PSD) of the synthesized motion signal according to Eq. (2.16) with the parameters in Table 2. Aside from the carrier frequency $f_c = 1$ Hz, where the PSD reaches its peak value, we also observe other frequency components in PSD distribution resulting from the modulation effect. The corresponding instantaneous amplitude and frequency are shown in Fig. 3. Here, we choose the period of amplitude modulation as $T_{am} = 1/f_{am} = 10$ s, which is in the same order as that observed in the following experimental results of a flexible cylinder in Section 4. The

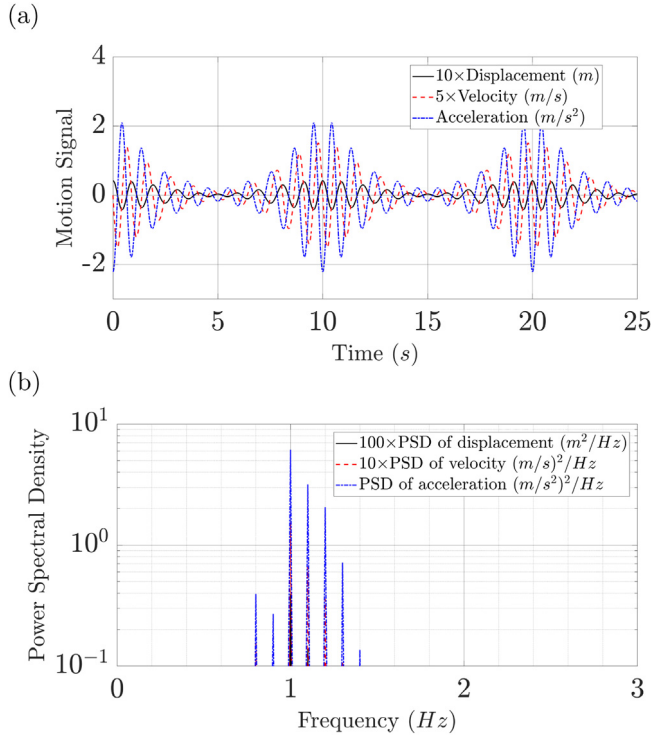


Fig. 2. The time history (a) and power spectral density (b) of the synthesized modulated motion signal (displacement, velocity, and acceleration) in Eq. (2.16).

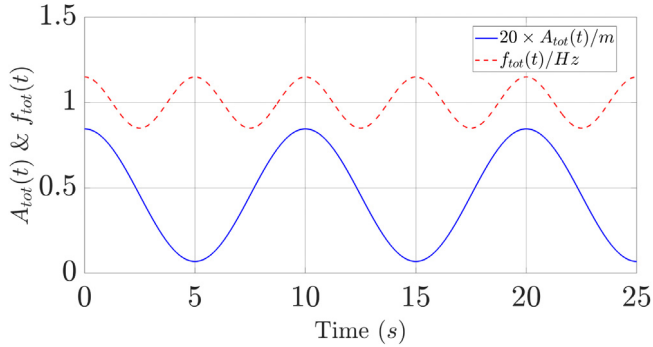


Fig. 3. The given instantaneous amplitude $A_{tot}(t)$ (envelope of the displacement) in Eq. (2.17a) and instantaneous frequency $f_{tot}(t)$ in Eq. (2.17b).

period of frequency modulation is chosen as a value different from that of amplitude modulation so as to analyze the relationship between identified hydrodynamic coefficients and the modulated motion.

According to the vortex-induced force decomposition method of the flexible cylinder described in the previous subsection, the force signal can be decomposed into the excitation force, $F_v(t) = \frac{\rho D l U^2}{2 v_0} CLe(t)\dot{y}(t)$, related to velocity and the added-mass force, $F_a(t) = -\frac{\rho \pi D^2 l}{4} CLa(t)\ddot{y}(t)$, related to acceleration. We call the sum of $F_v(t)$ and $F_a(t)$ as the reconstructed force using the following identified coefficients:

$$F_{Recon}(t) := F_v(t) + F_a(t) = \frac{\rho D l U^2}{2 v_0} CLe(t)\dot{y}(t) - \frac{\rho \pi D^2 l}{4} CLa(t)\ddot{y}(t). \quad (2.18)$$

In Eq. (2.18), $CLe(t)$ and $CLa(t)$ are called the time-varying excitation coefficients and added-mass coefficients for the elastically mounted cylinder under flow. Similar to the identification of vortex-induced force coefficients of the flexible cylinder, the sum of squared errors between the force signal reconstructed from the identified coefficients $F_{Recon}(t) =$

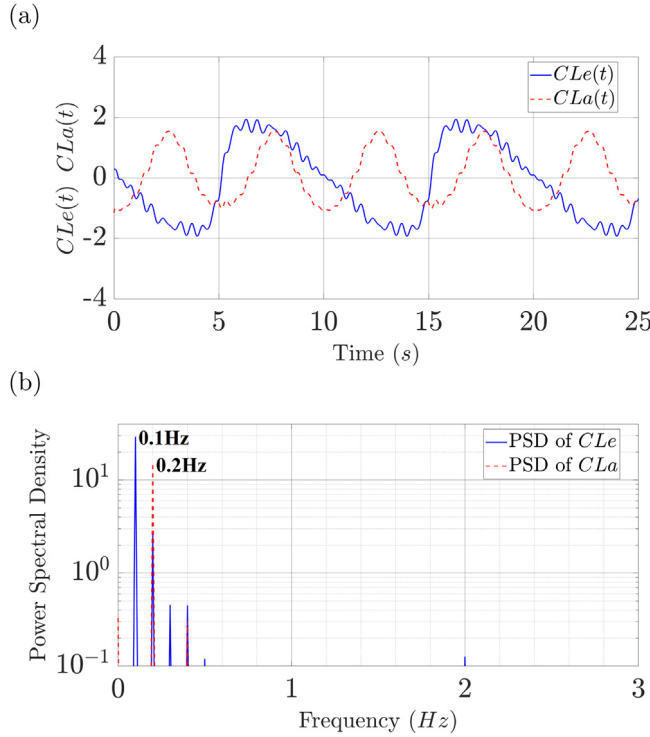


Fig. 4. The time history (a) and power spectral density (1/Hz) (b) of time-varying excitation coefficient and added-mass coefficient for modulated signal in Eq. (2.16).

$\frac{\rho D U^2}{2 v_0} CLe(t) \dot{y}(t) - \frac{\rho \pi D^2 l}{4} CLa(t) \ddot{y}(t)$, and the hydrodynamic force $F_{hydro}(t)$ in Eq. (2.15) should be minimized:

$$\min \sum_{i=1}^L [F_{hydro}(t_i) - F_{Recon}(t_i)]^2. \quad (2.19)$$

Namely, for any moment t_L , substituting the time history of $F_{hydro}(t)$ from the initial t_1 to the present t_L as \mathbf{f}_L and the time history of $\dot{y}(t)$, $\ddot{y}(t)$ from the initial moment t_1 to the present moment t_L as \mathbf{H}_L in Eq. (2.8), causes Eq. (2.14) to yield estimation of time-varying hydrodynamic coefficients $\hat{\theta}(L)$, which is $CLe(t)$, $CLa(t)$ at moment t_L . Repeating this process, we obtain the time history of hydrodynamic coefficients.

As shown in Fig. 4(a), the hydrodynamic coefficients obtained from Eq. (2.15) vary over time for a modulated motion in Eq. (2.16). The obtained time-varying excitation coefficient $CLe(t)$ has the same period as the instantaneous amplitude $A_{tot}(t)$ in Fig. 3, while the obtained time-varying added-mass coefficient $CLa(t)$ has the same period with the instantaneous frequency. This observation is further confirmed by Fig. 4(b), which shows that PSD of excitation coefficients and added-mass coefficients reach the peak value at 0.1 Hz and 0.2 Hz, respectively. This indicates that the excitation coefficient may contain the information of amplitude modulation and that the added-mass coefficient may contain the information of frequency modulation. This statement will be further discussed in the following subsection.

Time-varying hydrodynamic coefficients also capture the modulation information in the original hydrodynamic force accurately. Fig. 5 compares time history and PSD of the hydrodynamic force in Eq. (2.15), the reconstructed force $F_{Recon}(t)$ in Eq. (2.18) using time-varying coefficients, and the $F_{Recon}(t)$ using constant hydrodynamic coefficients $CLe_{LS} = 0.0209$ and $CLa_{LS} = -0.4168$ obtained from the Least Squares method. Time-varying coefficients are able to reconstruct the original hydrodynamic force acting on the cylinder accurately, while the time-invariant coefficients fail. Here, we note that PSD of hydrodynamic force F_{hydro} has larger values at 0.8 Hz and 1.2 Hz than that at the carrier frequency 1 Hz. This has likely resulted from the modulation effects.

To quantify the closeness between the original hydrodynamic force and the reconstructed one, we consider two kinds of coefficients of determination following the definition in equations (4) and (7) of Willett and Singer (1988):

$$R_W^2(L) := 1 - [(\hat{\mathbf{f}}_L - \hat{\mathbf{H}}_L \hat{\theta}(L))^T (\hat{\mathbf{f}}_L - \hat{\mathbf{H}}_L \hat{\theta}(L))] / [\hat{\mathbf{f}}_L^T \hat{\mathbf{f}}_L - \text{avg}(\hat{\mathbf{f}}_L)L], \quad \text{and} \quad (2.20a)$$

$$R_U^2(L) := 1 - [(\mathbf{f}_L - \mathbf{H}_L \hat{\theta}(L))^T (\mathbf{f}_L - \mathbf{H}_L \hat{\theta}(L))] / [\mathbf{f}_L^T \mathbf{f}_L - \text{avg}(\mathbf{f}_L)L], \quad (2.20b)$$

where $\text{avg}(\cdot)$ represents the average value of the inside vector. Both of these coefficients represent perfect fitting when they are equal to one. The first coefficient of determination $R_W^2(L)$ is equivalent to that of the ordinary least squares method

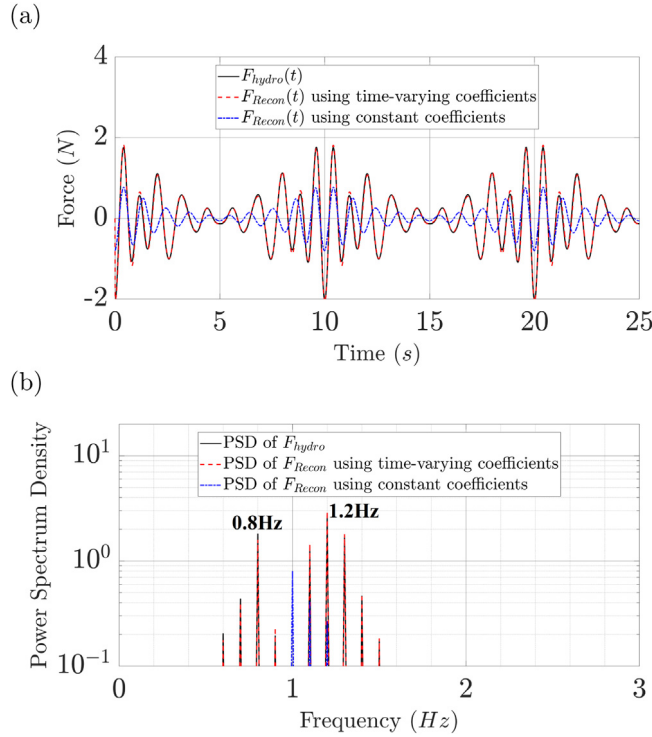


Fig. 5. A comparison of time history (a) and power spectral density (N^2/Hz) (b) of the hydrodynamic force $F_{\text{hydro}}(t)$, the reconstructed force $F_{\text{Recon}}(t)$ obtained from time-varying coefficient obtained by FF-LS method and $F_{\text{Recon}}(t)$ reconstructed from constant coefficients obtained by the least squares method.

with respect to the weighted fitting problem in Eq. (2.11), while Willett and Singer (1988) suggested that the second one $R_U^2(L)$ is more suitable for the weighted least squares method; e.g., FF-LS employed here. Fig. 7 shows these two types of coefficients of determination R_W^2 and R_U^2 as a function of time. The coefficient R_W^2 shows a periodic behavior with a value larger than 0.8 at $t \geq 5$ s, while the coefficient R_U^2 is approaching 1 as time increases. However, the normalized quantity such as coefficients of determination may result in misleading information (Draper, 1984; Kvålseth, 1985; Willett and Singer, 1988), and other dimensional quantities such as standard deviation may provide a more appropriate criteria of performance. A comprehensive performance analysis of FF-LS is a topic of ongoing works.

The resulting time-varying hydrodynamic coefficient provide the opportunities to describe the vortex-induced force as a linear time-varying feedback forcing on the structures; see Fig. 6. To utilize comprehensive analysis and synthesis frameworks in linear systems, approximating nonlinear system as a linear time-varying system is also employed in the control literature; see e.g., Tomás-Rodríguez and Banks (2003, 2010). Performing spectral analysis of the approximated linear system is also widely used to provide physical insight into observations of fluid problem; see e.g., DMD (Schmid, 2010), sparsity promoting DMD (Jovanović et al., 2014), or online DMD for time-varying system (Zhang et al., 2019). The FF-LS employed here is closely related to the online DMD, where the forgetting factor serves as the weighting factor in online DMD.

Typically, the vortex-induced force is modeled through a nonlinear wake model such as van der Pol oscillator; see e.g., Nayfeh et al. (2003), Facchinetti et al. (2004), Violette et al. (2007), Marzouk et al. (2007) and Akhtar et al. (2009). Recently, a time-varying nonlinear aerodynamics model has been developed (Li et al., 2019) using time-varying SINDy (Brunton et al., 2016) for a prototype bridge under time-varying mean wind speed, where the VIV feature shows a difference from that under stationary or steady wind. In this paper, we restrict the system parameters needed to be estimated as the time-varying excitation and added-mass coefficients and restrict our vortex-induced force as a linear combination of velocity and acceleration weighted with these time-varying coefficients; see Eq. (2.18). This restriction provides us physical interpretations of identified time-varying hydrodynamic coefficients, which are explored in the next section.

3. Predicting modulation using time-varying hydrodynamics

With the connection between time-varying hydrodynamic coefficients and modulation indicated in Section 2.2, we aim to predict the modulation using the obtained time-varying hydrodynamic coefficients. We first illustrate the prediction

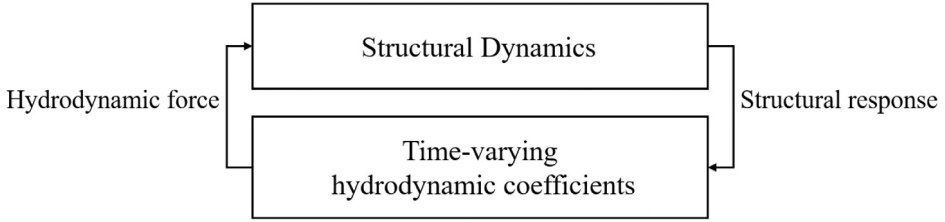


Fig. 6. The effect of identified time-varying hydrodynamic coefficients.

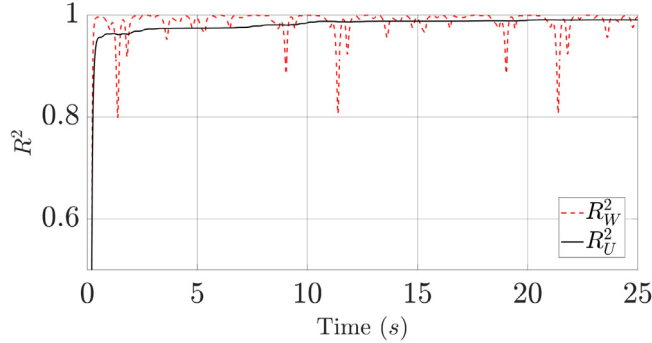


Fig. 7. Time history of coefficients of determination R_W^2 and R_U^2 using Eq. (2.20) for illustration example in Section 2.2.

method for an elastically mounted cylinder under flow (mass–spring–dashpot system), discussing the relationship between time-varying hydrodynamic coefficients and modulated VIV. Finally, we formalize the prediction method for a flexible cylinder.

3.1. Predicting modulation for an elastically mounted cylinder

Assuming that the identified time-varying coefficients are able to accurately reconstruct the hydrodynamic force acting on the cylinder (Fig. 5): $F_{\text{hydro}}(t) = F_{\text{Recon}}(t)$, we have the following equality using Eqs. (2.15) and (2.18):

$$m\ddot{y}(t) + c\dot{y}(t) + ky(t) = \frac{\rho DlU^2}{2v_0} CLe(t)\dot{y}(t) - \frac{\rho\pi D^2 l}{4} CLa(t)\ddot{y}(t). \quad (3.1)$$

Moving the right hand side of the Eq. (3.1) to its left hand side, we have:

$$[m + \frac{\rho\pi D^2 l}{4} CLa(t)]\ddot{y}(t) + [c - \frac{\rho DlU^2}{2v_0} CLe(t)]\dot{y}(t) + ky(t) = 0. \quad (3.2)$$

When the hydrodynamic coefficients vary over time, we can assume a non-trivial solution as a generalized form:

$$y(t) = \exp\left[\int_{t_0}^t \lambda(\tau)d\tau\right]y(t_0), \quad (3.3)$$

where the time-varying complex eigenvalue $\lambda(t)$ satisfying a generalized characteristic equation:

$$[m + \frac{\rho\pi D^2 l}{4} CLa(t)]\lambda(t)^2 + [c - \frac{\rho DlU^2}{2v_0} CLe(t)]\lambda(t) + k = 0 \quad (3.4)$$

assuming a time scale separation $|\frac{d\lambda(t)}{dt}| \ll |\lambda(t)^2|$. From Eq. (3.4), we can build the relationship between the time-varying eigenvalue and the time-varying coefficients through solving $\lambda(t)$:

$$\begin{aligned} \lambda_r(t) &= -\frac{c - \frac{\rho DlU^2}{2v_0} CLe(t)}{2[m + \frac{\rho\pi D^2 l}{4} CLa(t)]}, \\ \lambda_i(t) &= \sqrt{\frac{k}{[m + \frac{\rho\pi D^2 l}{4} CLa(t)]} - \lambda_r^2(t)}, \end{aligned} \quad (3.5)$$

where $\lambda_r(t)$ and $\lambda_i(t)$ are the real part and the imaginary part of the time-varying eigenvalue $\lambda(t)$, respectively.

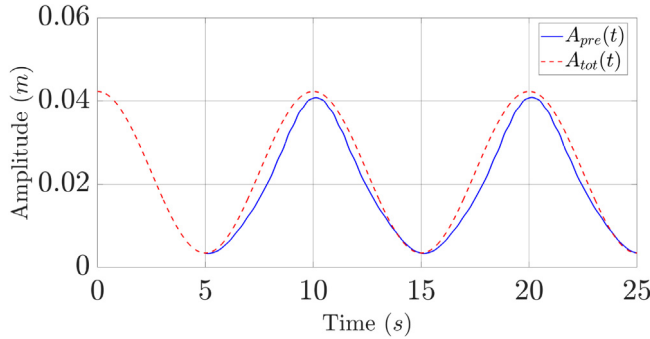


Fig. 8. A comparison between the predicted instantaneous amplitude (envelope of the displacement) using Eq. (3.8a) and that of the original signal given in Eq. (2.17a).

In an equivalent way, we can rewrite Eq. (3.2) into the state space $\mathbf{q} := [y(t) \quad \dot{y}(t)]^T$:

$$\frac{d\mathbf{q}}{dt} = \begin{bmatrix} 0 & 1 \\ \frac{-k}{m + \frac{\rho\pi D^2 l}{4} Cl_a(t)} & \frac{-c + \frac{\rho D l U^2}{2v_0} CLe(t)}{m + \frac{\rho\pi D^2 l}{4} Cl_a(t)} \end{bmatrix} \mathbf{q} =: \mathbf{A}(t)\mathbf{q}, \quad (3.6)$$

and compute the time-varying eigenvalues $\lambda(t)$ in Eq. (3.3) through computing the eigenvalues of matrix $\mathbf{A}(t)$.

Then, we build the relationship between the time-varying eigenvalue and the modulation comparing Eq. (3.3) with Eq. (2.16):

$$\exp[\int_{t_0}^t \lambda_r(\tau) d\tau] = \frac{A_c + m(t)}{A_c + m(t_0)} = \frac{A_{tot}(t)}{A_{tot}(t_0)}, \quad (3.7a)$$

$$\lambda_i(t) = 2\pi[f_c + f_m(t)] = 2\pi f_{tot}(t). \quad (3.7b)$$

Using Eq. (3.7), we predict the corresponding instantaneous amplitude $A_{pre}(t)$ and frequency $f_{pre}(t)$:

$$A_{pre}(t) = \exp[\int_{t_0}^t \operatorname{Re}[\lambda_{pre}(\tau)] d\tau] A_{pre}(t_0), \quad (3.8a)$$

$$f_{pre}(t) = |\operatorname{Im}[\lambda_{pre}(t)]|/(2\pi), \quad (3.8b)$$

where we denote the eigenvalues predicted using Eq. (3.5) or $\operatorname{eig}[\mathbf{A}(t)]$ with identified time-varying hydrodynamic coefficients in Section 2 as $\lambda_{pre}(t)$.

The modulation prediction method with identified time-varying coefficients here works well for predicting both the instantaneous amplitude and frequency. Fig. 8 compares the predicted amplitude using Eq. (3.8a) with the given instantaneous amplitude in Eq. (2.17b), and they are close to each other. Here, we choose $t_0 = 5$ s in that the initial identified time-varying coefficients in Fig. 4 is related to the initial guess value and is not reflecting the system dynamics.

Fig. 9 compares the predicted frequency using Eq. (3.8b) with the given instantaneous frequency in Eq. (2.17b), and they are close. However, we can observe that the predicted frequency lags behind the given instantaneous frequency in Eq. (3.8b). This results from the fact that we only use the information before the current instant t_l in FF-LS to estimate time-varying hydrodynamic coefficients $\theta(L)$. Using the information both before and after the current instant may provide results without any time-delay. This time-delay effect in estimated hydrodynamic coefficients using FF-LS may be also related to the underestimation of amplitude shown in Fig. 8.

3.2. Relationship between the time-varying hydrodynamics and modulated VIV

In the subsection above, we use the time-varying coefficient to predict instantaneous amplitude and frequency. The results also provide a hint to explain the physical meaning of the time-varying hydrodynamic coefficients. When hydrodynamic coefficients become time-invariant, it is trivial that no modulation exists and that motion becomes sinusoidal with exponential growth or decay: $y(t) = e^{\lambda(t-t_0)}y(t_0)$.

If modulation exists, we have the relationship between the instantaneous amplitude and frequency and time-varying hydrodynamic coefficients using Eqs. (3.5) and (3.7):

$$\frac{\rho D l U^2}{2v_0} CLe(t) = \frac{2k \frac{dA_{tot}(t)/dt}{A_{tot}(t)}}{[2\pi f_{tot}(t)]^2 + [\frac{dA_{tot}(t)/dt}{A_{tot}(t)}]^2} + c, \quad (3.9a)$$

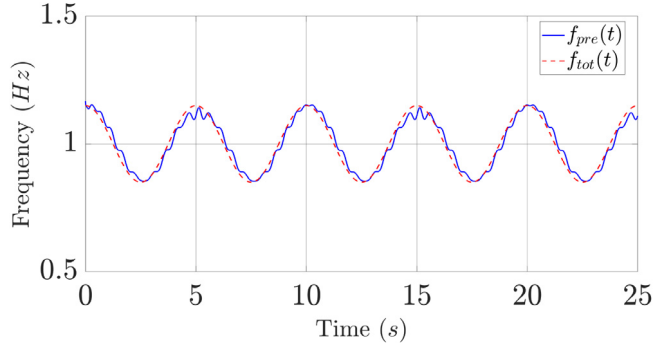


Fig. 9. A comparison between predicted instantaneous frequency using Eq. (3.8b) and that of original signal given in Eq. (2.17b).

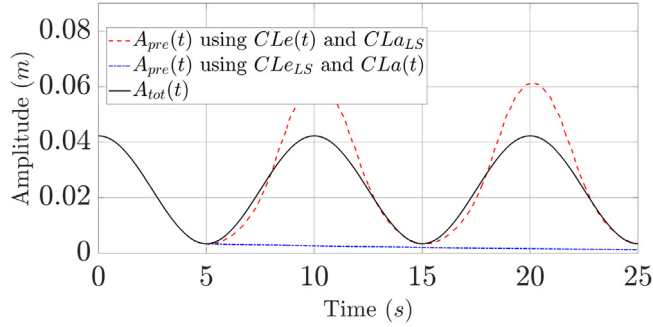


Fig. 10. A comparison among predicted instantaneous amplitude (envelope of the displacement) using $CLe(t)$ and CLa_{LS} , the predicted instantaneous amplitude using CLe_{LS} and $CLa(t)$, and that of the original signal given in Eq. (2.17a).

$$\frac{\rho\pi D^2 l}{4} CLa(t) = \frac{k}{[2\pi f_{tot}(t)]^2 + [\frac{dA_{tot}(t)/dt}{A_{tot}(t)}]^2} - m. \quad (3.9b)$$

From these equations, we can see that the time-varying hydrodynamic coefficients contain both amplitude modulation and frequency modulation information.

Here, we investigate the effects of time-varying hydrodynamic coefficients on predicting modulation through treating one hydrodynamic coefficient as a time-invariant value obtained using the least squares method. In Figs. 10 and 11, we compare the instantaneous amplitude and frequency predicted using time-varying excitation coefficient $CLe(t)$ and constant added-mass coefficient CLa_{LS} (the red dashed lines), results predicted using constant excitation coefficient CLe_{LS} and time-varying added-mass coefficient $CLa(t)$ (the blue dash dot lines), and those of the original signal given in Eq. (2.17a) (the black solid lines).

Amplitude modulation has a closer connection to the excitation coefficient. Fig. 10 indicates that the time-varying excitation coefficient $CLe(t)$ and the constant added-mass coefficient CLa_{LS} also predict the amplitude modulation phenomenon, but perhaps not in the correct magnitude. However, the constant excitation coefficient CLe_{LS} and the time-varying added-mass coefficient $CLa(t)$ predict the amplitude like exponential decaying. This phenomenon may be explained from Eq. (3.9a).

If no amplitude modulation exists: $dA_{tot}(t)/dt = 0$, the excitation coefficients do not vary over time according to Eq. (3.9a); i.e., amplitude modulation is necessary for the time-varying excitation coefficient. Furthermore, the sign of the temporal derivative of instantaneous amplitude $dA_{tot}(t)/dt$ determines the sign of the excitation coefficients as indicated in Eq. (3.9a) if structural damping is negligible; e.g., $\xi = \frac{c}{2\sqrt{mk}} = 0.15\%$ here. Thus, periodic excitation coefficient provides the amplitude modulation, and in contrast, a constant excitation coefficient predicts the amplitude like exponential decaying/growth as shown in Fig. 10. This further indicates that considering the influence of $dA_{tot}(t)/dt$ on the excitation coefficients is critical to improve the qualitative property of excitation coefficients and the prediction for amplitude modulation. The analysis here provides theoretical support for similar suggestion in Section 4.

On the other hand, added-mass coefficient has a closer connection to the frequency modulation. In Fig. 11, obvious frequency modulation disappears when predicted using the time-varying excitation $CLe(t)$ coefficient with the constant added-mass coefficient CLa_{LS} . However, the constant excitation coefficient CLe_{LS} and the time-varying added-mass coefficients $CLa(t)$ also predict frequency modulation close to that of the given signal in Eq. (2.17a).

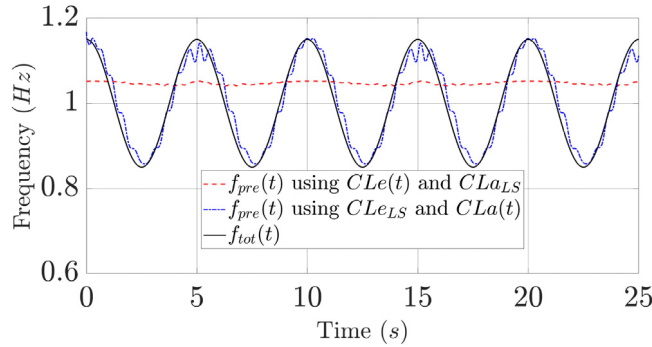


Fig. 11. A comparison among predicted instantaneous frequency using $CLe(t)$ and CLa_{LS} , the predicted instantaneous frequency using CLe_{LS} and $CLa(t)$, and that of the original signal given in Eq. (2.17b).

To explain these effects, we rewrite Eqs. (3.9a) and (3.9b) in another direction:

$$A_{pre}(t) = \exp\left[\int_{t_0}^t -\frac{c - \frac{\rho DU^2}{2v_0} CLe(\tau)}{2[m + \frac{\rho\pi D^2 l}{4} CLa(\tau)]} d\tau\right] A_{pre}(t_0), \quad (3.10a)$$

$$f_{pre}(t) = \frac{1}{2\pi} \sqrt{\frac{k}{[m + \frac{\rho\pi D^2 l}{4} CLa(t)]}} \sqrt{1 - \frac{[c - \frac{\rho DU^2}{2v_0} CLe(t)]^2}{4k[m + \frac{\rho\pi D^2 l}{4} CLa(t)]}}, \quad (3.10b)$$

which provides the instantaneous amplitude and frequency from the time-varying hydrodynamic coefficients.

The instantaneous frequency is dominated by the time-varying added-mass coefficients. In Eq. (3.10b), the time-varying excitation coefficients only appear in term $\sqrt{1 - \frac{[c - \frac{\rho DU^2}{2v_0} CLe(t)]^2}{4k[m + \frac{\rho\pi D^2 l}{4} CLa(t)]}}$. This term is in the range of [0.9882, 1] in this example, resulting in $f_{pre}(t) \approx \frac{1}{2\pi} \sqrt{\frac{k}{[m + \frac{\rho\pi D^2 l}{4} CLa(t)]}}$. Thus, if we replace the time-varying excitation coefficient $CLe(t)$ as a constant one CLe_{LS} , the predicted frequency is also close to the given frequency as shown in Fig. 11. However, when we replace the time-varying added-mass coefficient $CLa(t)$ as a constant one CLa_{LS} , the obvious frequency modulation disappears.

Both numerical and analytical results here reveal the physics insight of time-varying hydrodynamic coefficients and the hydrodynamic mechanism behind the modulated VIV; i.e., the time-varying excitation coefficients mainly influence the amplitude modulation, and the time-varying added-mass coefficients contain the major information of frequency modulation.

3.3. Predicting modulation for a flexible cylinder

Then, we extend the modulation prediction method from an elastically mounted cylinder to a flexible cylinder. Here, the prediction method for a horizontally placed flexible cylinder includes both the time-varying added-mass coefficients and time-varying excitation coefficients, which generalizes the method of Liu et al. (2018). Similarly, assuming that the vortex-induced force $f_{CF}(z, t)$ reconstructed from the time-varying coefficients are accurate, we have the forced Euler–Bernoulli beam equation:

$$\begin{aligned} m \frac{\partial^2 y(z, t)}{\partial t^2} + c \frac{\partial y(z, t)}{\partial t} + \frac{\partial}{\partial z^2} [EI \frac{\partial^2 y(z, t)}{\partial z^2}] - F_T(z, t) \frac{\partial^2 y(z, t)}{\partial z^2} &= f_{CF}(z, t)/l \\ &= \frac{\rho D U_{RMS}^2(z, t)}{2v_0(z)} CLe(z, t) \frac{\partial y}{\partial t}(z, t) - \frac{\rho\pi D^2}{4} CLa(z, t) \frac{\partial^2 y}{\partial t^2}(z, t). \end{aligned} \quad (3.11)$$

In this equation, m is the mass per unit length; c is the structural damping factor in air; EI is the bending stiffness, and $F_T(z, t)$ is the tension at the ends of the cylinder.

Moving the right hand side of Eq. (3.11) to its left hand side, the original equation is rewritten as:

$$\begin{aligned} [m + \frac{\rho\pi D^2}{4} CLa(z, t)] \frac{\partial^2 y(z, t)}{\partial t^2} + [c - \frac{\rho D U_{RMS}^2(z, t)}{2v_0(z)} CLe(z, t)] \frac{\partial y(z, t)}{\partial t} \\ + \frac{\partial^2}{\partial z^2} [EI \frac{\partial^2 y(z, t)}{\partial z^2}] - F_T(z, t) \frac{\partial^2 y(z, t)}{\partial z^2} = 0. \end{aligned} \quad (3.12)$$

Table 3

The parameters of a flexible cylinder under oscillatory flow.

Parameters	Value	Parameters	Value
Hydrodynamic diameter D (m)	0.024	Axial stiffness EA (N)	6.67×10^5
Length L (m)	4	Bending stiffness EI (N m ²)	10.5
Mass per unit length m_s (kg/m)	0.69	Pretension F_{T_0} (N)	500
1 st natural frequency f_1 (Hz)	2.68	2 nd natural frequency f_2 (Hz)	5.46

Here, we consider the hinge boundary condition that is commonly used in model tests (Fu et al., 2014; Song et al., 2016a):

$$y(z=0, t) = y(z=L, t) = \frac{\partial^2}{\partial z^2}y(z=0, t) = \frac{\partial^2}{\partial z^2}y(z=L, t) = 0. \quad (3.13)$$

Trying to cast Eq. (3.12) into an eigenvalue problem, we use the Galerkin method, which expresses the solution on the basis functions that satisfy boundary conditions:

$$y(z, t) = \sum_{k=1}^n \hat{y}_k(t) \sin(k \frac{z\pi}{L}), \quad (3.14)$$

where L represents the length of the flexible cylinder. Defining the motion vector $\hat{\mathbf{y}}(t)$:

$$[\hat{\mathbf{y}}]_k(t) := \hat{y}_k(t), \quad k = 1, 2, \dots, n, \quad (3.15)$$

we can rewrite Eq. (3.12) as:

$$\hat{\mathbf{M}}(t) \frac{\partial^2}{\partial t^2} \hat{\mathbf{y}}(t) + \hat{\mathbf{C}}(t) \frac{\partial}{\partial t} \hat{\mathbf{y}}(t) + \hat{\mathbf{K}}(t) \hat{\mathbf{y}}(t) = \mathbf{0}, \quad (3.16)$$

using the $\hat{\mathbf{M}}(t)$, $\hat{\mathbf{C}}(t)$ and $\hat{\mathbf{K}}(t)$ described in Appendix B. It can be written into the state variable form similar to Eq. (3.6):

$$\frac{d}{dt} \begin{bmatrix} \hat{\mathbf{y}}(t) \\ \frac{d}{dt} \hat{\mathbf{y}}(t) \end{bmatrix} = \begin{bmatrix} \mathbf{0} & \mathbf{I}_{n \times n} \\ -\hat{\mathbf{M}}^{-1}(t)\hat{\mathbf{K}}(t) & -\hat{\mathbf{M}}^{-1}(t)\hat{\mathbf{C}}(t) \end{bmatrix} \begin{bmatrix} \hat{\mathbf{y}}(t) \\ \frac{d}{dt} \hat{\mathbf{y}}(t) \end{bmatrix} =: \hat{\mathbf{A}}(t) \begin{bmatrix} \hat{\mathbf{y}}(t) \\ \frac{d}{dt} \hat{\mathbf{y}}(t) \end{bmatrix}, \quad (3.17)$$

where $\mathbf{I}_{n \times n}$ is an identity matrix with their sizes indicated by their subscripts, and we assume $\hat{\mathbf{M}}(t)$ is invertible.

Similar to Eqs. (3.8a) and (3.8b), the eigenvalues of $\hat{\mathbf{A}}(t)$: $\lambda_{pre,i} := \text{eig}(\hat{\mathbf{A}}(t))$ can be used to determine the instantaneous amplitude and frequency of the modulated vortex-induced vibrations:

$$A_{pre,i}(t) = \exp \left[\int_{t_0}^t \text{Re}[\lambda_{pre,i}(\tau)] d\tau \right] A_{pre,i}(t_0), \quad (3.18a)$$

$$f_{pre,i}(t) = |\text{Im}[\lambda_{pre,i}(t)]|/(2\pi). \quad (3.18b)$$

Here, $A_{pre,i}(t)$, $A_{pre,i}(t_0)$ and $f_{pre,i}$ should be understood as the instantaneous amplitude and frequency under the basis function coordinates: $\sin(k \frac{z\pi}{L})$, $k = 1, 2, \dots, n$.

Here, we note that the time-varying effect of excitation and added-mass coefficients are combined into the time-varying effect of the damping matrix $\hat{\mathbf{C}}(t)$ and the mass matrix $\hat{\mathbf{M}}(t)$, respectively. Under vertical or catenary configuration, the tension $F_T(z, t)$ of a riser is a function of spatial location due to gravity, and $F_T(z, t)$ is typically a function of time leading to the frequency modulation phenomenon; see e.g., Franzini et al. (2009), da Silveira et al. (2009) and Franzini et al. (2010, 2015a,b, 2018). The time-varying effect of tension will lead to the time-varying effect of the stiffness matrix $\hat{\mathbf{K}}(t)$, which also fits into the current analysis framework. In the next section, we will employ the identification method in Section 2 and the prediction method in Section 3 to the experimental data of a flexible cylinder under modulated VIV.

4. Hydrodynamics of a highly tensioned flexible cylinder under modulated VIV

4.1. Model test

The experiments were performed in the Ocean Engineering Basin in Shanghai Jiao Tong University, where the entire experimental device was installed under the bottom of the carriage. This experimental device, called a 'forced oscillation device', contains two horizontal tracks and two vertical tracks, which enable the cylinder model to move as a given trajectory. The two ends of the cylinder were connected to this forced oscillation device with universal joints, and a constant pre-tension was maintained. The experimental setup is shown in Fig. 12.

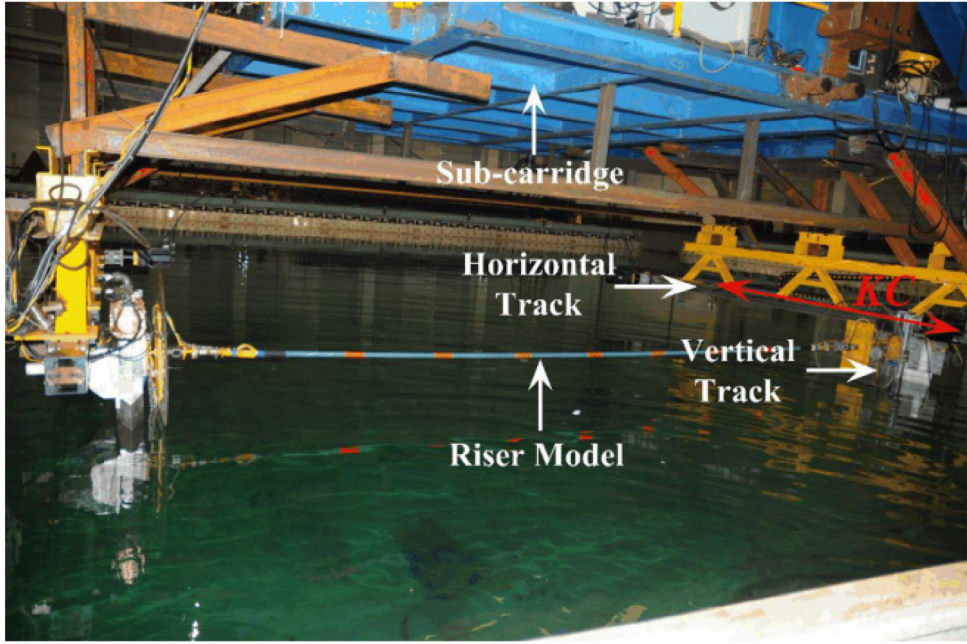


Fig. 12. The testing setup for a flexible cylinder under oscillatory flow.

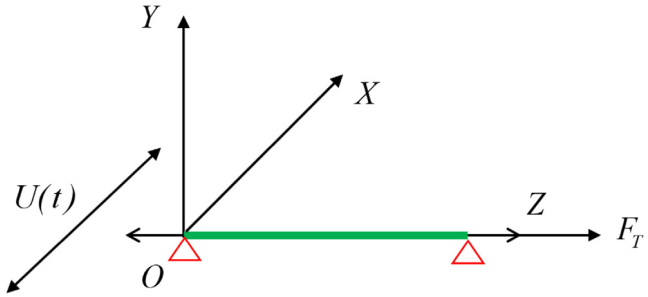


Fig. 13. A submerged flexible cylinder with tension force under oscillatory flow.

The experimental parameters are shown in [Table 3](#), where the hydrodynamic diameter of a scaled riser was 24 mm with an effective length of 4 m. In this table, the nth natural frequency in still water is calculated according to vibration theory of the simply-supported beam:

$$f_n(t) = \frac{n}{2L} \sqrt{\frac{F_{T_0}}{m} + \frac{n^2 \pi^2 EI}{L^2}}, \quad m = m_S + m_A, \quad n = 1, 2, 3, \dots . \quad (4.1)$$

In this equation, n is the order of natural frequency, L is the length of the cylinder, F_{T_0} is pretension force, EI is the bending stiffness of riser, and m is the total mass per unit length, which equals to the sum of the structural mass m_S and added-mass m_A . Here, we use the added-mass concept originally born in the ideal flow to represent force that is related to the acceleration, thereby providing added inertial effect on the structure. The added-mass coefficient in Eq. (4.1) is chosen as the unit value, which is the value of an oscillating cylinder in ideal inviscid flow. This value is different from the added-mass coefficients measured in the viscous flow ([Gopalkrishnan, 1993](#); [Vikestad et al., 2000](#); [Sarpkaya, 2010](#); [Song et al., 2016a](#)), but provides an initial estimation of the structural natural frequency.

During the model test, the flexible cylinder was forced to harmonically oscillate in the horizontal direction with a given amplitude and period. This forced oscillation generates oscillatory flow relative to the central axis of the cylinder in the horizontal direction as shown in [Fig. 13](#). This horizontal direction is denoted as the IL direction (X axis in [Fig. 13](#)), and the vertical direction is denoted as the CF direction (Y axis in [Fig. 13](#)). The central axis of the cylinder lies on the Z-axis. In this experiment, we do not impose a constant towing speed which is typically used to investigate the VIV of a flexible cylinder under uniform flow; e.g., [Song et al. \(2016b\)](#).

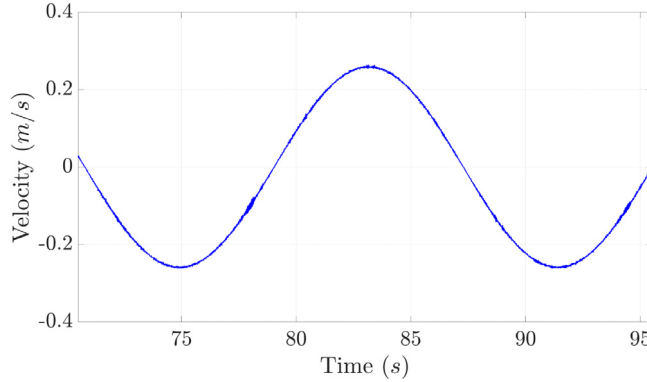


Fig. 14. The time history of the relative oscillatory flow velocity ($A_{osi} = 0.68$ m, $T_{osi} = 16.5$ s).

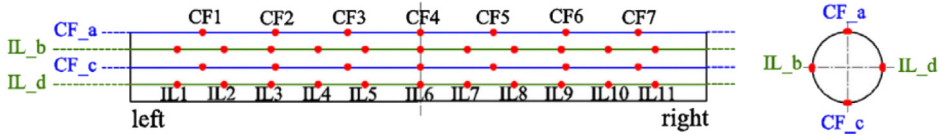


Fig. 15. The arrangement of strain gauges on the surface of the cylinder model.

The generated oscillatory flow velocity relative to the cylinder can be expressed as: $U(t) = A_{osi} \frac{2\pi}{T_{osi}} \cos(\frac{2\pi}{T_{osi}} t)$, whose time history with $A_{osi} = 0.68$ m, $T_{osi} = 16.5$ s is shown in Fig. 14. Here, A_{osi} denotes the maximum oscillating amplitude, and T_{osi} means the oscillatory period. The corresponding parameters of oscillatory flow, the Keulegan–Carpenter (KC) number (Keulegan and Carpenter, 1958) with respect to the imposed oscillatory motion and reduced velocity, are defined as:

$$KC = \frac{2\pi A_{osi}}{D}, \quad (4.2a)$$

$$V_r(t) = \frac{U(t)}{f_1 D}. \quad (4.2b)$$

D is the hydrodynamic diameter of the flexible cylinder, and f_1 denotes the first natural frequency of the test model in still water. More details of the experimental model test are included in Fu et al. (2014) and Wang et al. (2015a). In the following analysis, we only focus on the $A_{osi} = 0.68$ m, $T_{osi} = 16.5$ s case where the modulation phenomenon is most obvious.

In the experiment, Fiber Bragg Grating (FBG) strain sensors were used to measure the strain response of the cylinder model. The FBG strain sensors were arranged in the CF_a, CF_c, IL_b and IL_d directions of the cylinder model and were used to measure the strain in these four directions of the model, namely ϵ_{CF_a} , ϵ_{CF_c} , ϵ_{IL_b} and ϵ_{IL_d} , which are shown in Fig. 15. A total of 36 (FBG) strain sensors were instrumented on the surface of the cylinder model in both the CF and IL directions to capture VIV response. As shown in Fig. 15, lines CF_a and CF_c along the CF direction were symmetric with respect to the neutral layer of the model, while lines IL_b and IL_d belong to the IL direction. All of the strain signals were synchronously acquired at a rate of 250 Hz.

4.2. Response and vortex-induced force of modulated VIV

For a flexible cylinder under the relative oscillatory flow generated by the forced oscillation as described above, the vortex-induced vibration was observed (Fu et al., 2014; Wang et al., 2015a). The observed VIV under this oscillatory flow showed different features from the VIV under steady flow, such as amplitude modulation and time-sharing (frequency modulation) effect.

The bending displacement in the IL and CF directions can be obtained indirectly from the bending strain measured at the cylinder surface using modal analysis (Lie and Kaasen, 2006). Appendix C shows the preprocessing of bending strain and modal analysis to obtain VIV displacements of the cylinder in the CF and IL directions. Alternatively, the displacement can also be obtained directly through optical tracking technique; see e.g., Pereira et al. (2013), Pesce et al. (2017) and Franzini et al. (2015b, 2018). With obtained VIV displacement, the vortex-induced force can be reconstructed through the inverse analysis (Song et al., 2016a). Different from computing structure response under certain hydrodynamic force as shown in Fig. 6, the inverse analysis compute the hydrodynamic force according to measured structural response and structural dynamics as shown in Fig. 16. The hydrodynamic force acting on the flexible cylinder is computed according

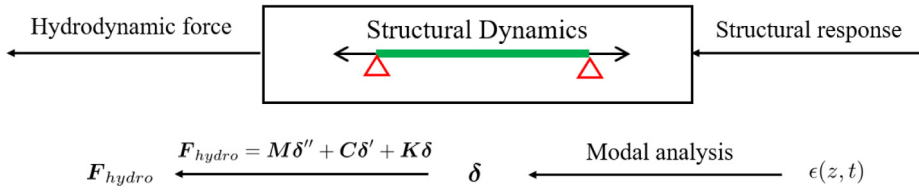


Fig. 16. Illustration of inverse analysis to obtain hydrodynamic force from structural response.

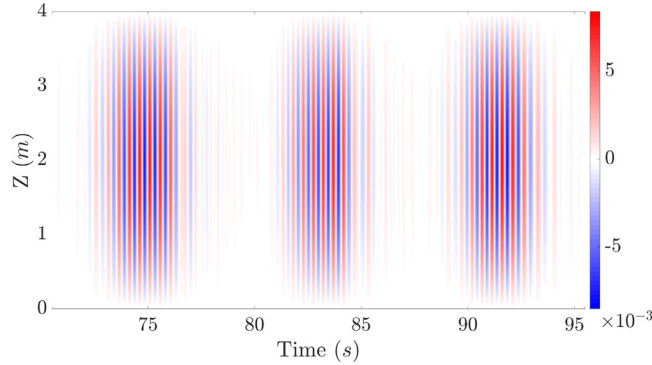


Fig. 17. The time–space distribution of VIV displacement (m) ($A_{osi} = 0.68$ m, $T_{osi} = 16.5$ s, $KC = 178$ and $\max(Vr) = 4$).

the finite element model of a beam:

$$\mathbf{F}_{hydro} = \mathbf{M}\delta'' + \mathbf{C}\delta' + \mathbf{K}\delta, \quad (4.3)$$

where \mathbf{M} , \mathbf{C} and \mathbf{K} are the global mass matrix, damping matrix, and stiffness matrix of the cylinder, respectively; δ , δ' , and δ'' are the displacement vector, velocity vector, and acceleration vector, respectively. The velocity vector δ' and the acceleration vector δ'' are obtained using the central-difference method to calculate the first-order and second-order time derivatives of δ . \mathbf{F}_{hydro} is the hydrodynamic force vector. For a riser with N nodes and six degree of freedom at each node, the dimensions of \mathbf{M} , \mathbf{C} , and \mathbf{K} are $6N \times 6N$, and the dimensions of δ and \mathbf{F}_{hydro} are $6N \times 1$.

The stiffness matrix \mathbf{K} of the cylinder with a tensional force includes two parts: $\mathbf{K} = \mathbf{K}_a^e + \mathbf{K}_b^e$, where \mathbf{K}_a^e is the prestressed stiffness matrix caused by axial tension in the cylinder, and \mathbf{K}_b^e is the small displacement linear stiffness matrix caused by the cylinder bending stiffness. The Rayleigh damping model offers the damping matrix \mathbf{C} of the cylinder: $\mathbf{C} = \alpha\mathbf{M} + \beta\mathbf{K}$, where α and β are the Rayleigh damping coefficients, which can be derived by the natural frequency and structural damping ratio of the cylinder. The displacement vector δ of the cylinder can be expressed as: $\delta = [\delta_1^T \ \delta_2^T \ \dots \ \delta_N^T]^T$, ($i = 1, 2, \dots, N$), where N is the node number. Universal joints are used at the two ends of the cylinder to constrain any twisting. Tension variation caused by axial elongation is relatively small compared to pretension 500N, and the spatial variation of tension resulting from gravity is also negligible considering horizontal configuration. As a result, we consider the tension $F_T(z, t) = F_{T_0} = 500$ N as a constant value in this paper. Including tension variation into consideration will be a promising direction of future work.

The matrices \mathbf{M} , \mathbf{C} , and \mathbf{K} employed here are obtained based on finite element model, and they are different from $\hat{\mathbf{M}}$, $\hat{\mathbf{C}}$, and $\hat{\mathbf{K}}$ derived from Fourier Galerkin method in Section 3.3 and Appendix B. Instead of Fourier Galerkin projection, we employ finite element model in Eq. (4.3) to obtain hydrodynamic force that is consistent with Song et al. (2016a), Zhang et al. (2018) and Liu et al. (2018). Moreover, reconstructed hydrodynamic force includes the first and higher order modes. Nevertheless, we employ the Fourier Galerkin method to predict modulation in Section 3.3 so as to establish a closer connection between flexible cylinder and elastically mounted rigid cylinder. A comprehensive framework based on the Galerkin projection is the direction of ongoing work.

After obtaining the structural response vectors δ , δ' , and δ'' with the mass matrix \mathbf{M} , the stiffness matrix \mathbf{K} and the damping matrix \mathbf{C} , the inverse analysis gives the hydrodynamic force \mathbf{F}_{hydro} according to Eq. (4.3). We refer to the Appendix A of Song et al. (2016a) for the accuracy analysis of this inverse analysis for hydrodynamic force identification. In the following analysis, we focus on the hydrodynamic force in the CF direction (Y-direction) and denote the hydrodynamic force component in this direction as f_{CF} .

Under oscillatory flow, both the VIV response and the vortex-induced force depict the amplitude and frequency modulations phenomena. Fig. 17 is the time–space distribution of obtained VIV displacement through the modal analysis method, and the first order mode vibration is dominant in this experimental condition. Fig. 18 depicts the time history

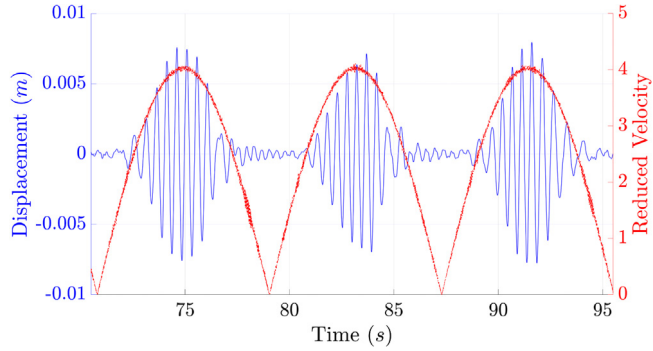


Fig. 18. The time history of VIV displacement at the midpoint of the cylinder ($A_{osi} = 0.68$ m, $T_{osi} = 16.5$ s, $KC = 178$ and $\max(V_r) = 4$).

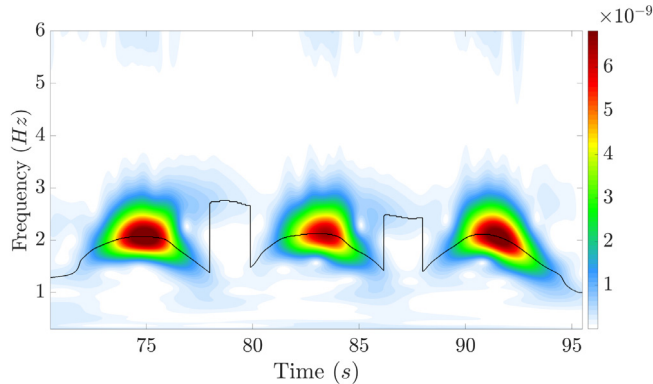


Fig. 19. The wavelet analysis of VIV strain at the midpoint of the cylinder ($A_{osi} = 0.68$ m, $T_{osi} = 16.5$ s, $KC = 178$ and $\max(V_r) = 4$) (the black line: Response dominant frequency).

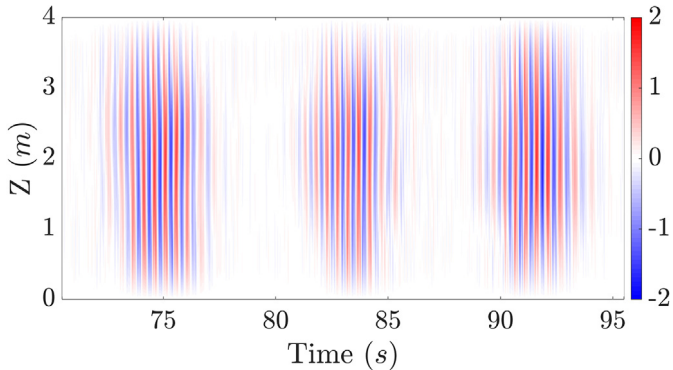


Fig. 20. The time–space distribution of vortex-induced force (N/m) ($A_{osi} = 0.68$ m, $T_{osi} = 16.5$ s, $KC = 178$ and $\max(V_r) = 4$).

of VIV displacement at the midpoint of the cylinder. These results indicate that amplitude modulation occurs in vortex-induced vibrations of a flexible cylinder under oscillatory flow (Fu et al., 2013, 2014), and the VIV developing process including ‘building-up’, ‘lock-in’ and ‘dying-out’ is proposed. Fig. 19 depicts wavelet analysis results of bending strain at the midpoint of the cylinder (the black lines denote the dominant frequency varying over time). The wavelet analysis shows that the VIV of the flexible cylinder under oscillatory flow has a frequency modulation effect, which means that vibration frequency changes over time. Figs. 20 and 21 represent the time–space distribution and the time history of vortex-induced force obtained through inverse analysis, respectively. These results show that the vortex-induced force of the flexible cylinder under oscillatory flow has similar modulation feature to response, and the first order mode vibration is also dominant for hydrodynamic force in this experimental condition.

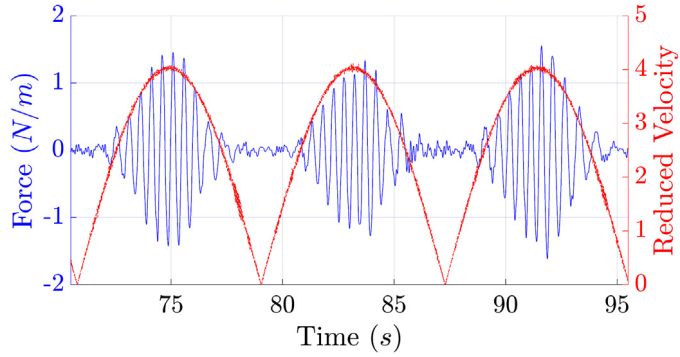


Fig. 21. The time history of vortex-induced force at the midpoint of the cylinder ($A_{osi} = 0.68 \text{ m}$, $T_{osi} = 16.5 \text{ s}$, $KC = 178$ and $\max(Vr) = 4$).

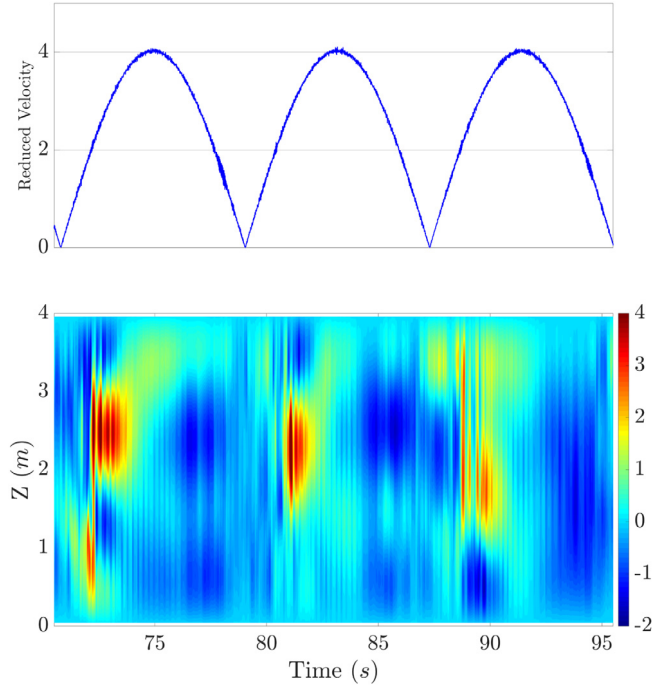


Fig. 22. The time–space distribution of the identified excitation coefficients $CLe(z, t)$ of the cylinder.

4.3. The time-varying hydrodynamic coefficients under modulated VIV

After obtaining vortex-induced force and the VIV response, corresponding time-varying vortex-induced force coefficients, namely the excitation coefficients and the added-mass coefficients, are identified through the Forgetting Factor Least Squares method described in Section 2. Namely, for any moment t_L , substituting the time history of f_{CF} from t_1 to t_L as \mathbf{f}_L and the time history of $\dot{y}(z, t)$, $\ddot{y}(z, t)$ from the initial moment t_1 to the present moment t_L as \mathbf{H}_L in Eq. (2.8), causes Eq. (2.14) to yield results of $\hat{\theta}(L)$, which provide estimation of $CLe(z, t)$, $ClA(z, t)$ at moment t_L at a specific location z . Repeating above process for all moments and all locations of the cylinder, we get the time–space distribution of the hydrodynamic coefficients. For validation of identifying hydrodynamic coefficients of a flexible cylinder under steady VIV, we refer to Appendix A of Liu et al. (2018).

Under modulated vortex-induced vibration, VIV excitation coefficients also show time-varying characteristics. Fig. 22 provides the time–space distribution of the identified excitation coefficient $CLe(z, t)$ of the flexible cylinder, and Fig. 23 gives the time history of excitation coefficient at the midpoint of the cylinder $CLe(z_{mid}, t)$. The excitation coefficient at the midpoint of the cylinder grows rapidly when the reduced velocity reaches a certain value (in this case, when the reduced velocity reach 2.5, as shown in Fig. 23). When reduced velocity reaches the maximum value, the excitation coefficient at the midpoint of the cylinder decreases to zero. During the falling edge of the reduced velocity, the excitation coefficient at the mid region decreases to a minus value and recovers slowly to zero. These results and the trend of excitation coefficient

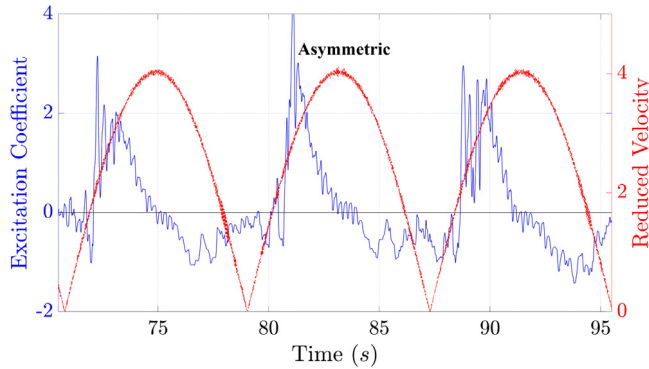


Fig. 23. The time history of the identified instantaneous excitation coefficients at the midpoint of the cylinder $CLe(z_{mid}, t)$.

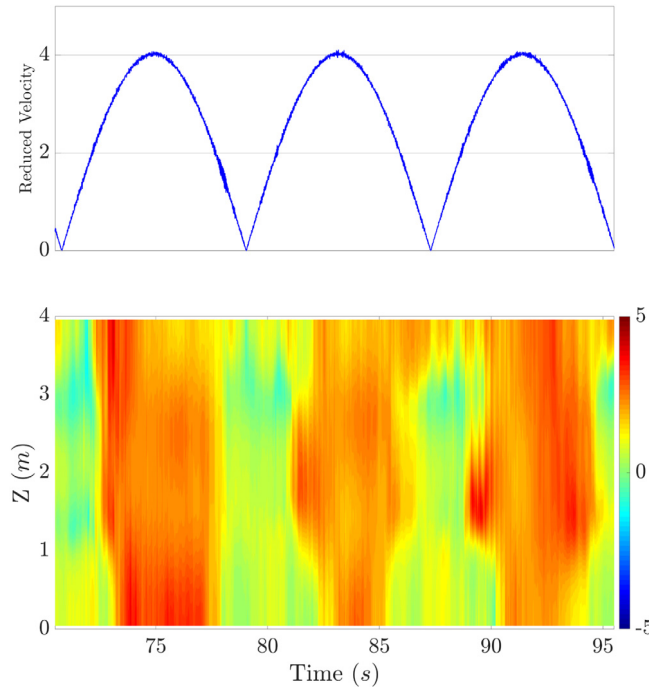


Fig. 24. The time–space distribution of the identified added-mass coefficients $CLa(z, t)$ of the cylinder.

explained the hydrodynamic mechanism behind ‘building-up’, ‘lock-in’ and ‘dying-out’ processes of the VIV developing (Fu et al., 2014). For the second cycle in Fig. 23, the time history of excitation coefficients appears as a larger peak value compared with other cycles. This phenomenon may be related to the observation that the maximum displacement of the second cycle shown in Fig. 18 is behind the instant when reduced velocity is largest, while the other two cycles shows the maximum displacement and reduced velocity at almost the same instant. We will further discuss the effects of time-varying excitation coefficients on amplitude modulation in the next subsection.

The added-mass coefficient also varies over time during different processes of the modulated VIV. Fig. 24 depicts the time–space distribution of the identified added-mass coefficients $CLa(z, t)$ of the flexible cylinder, and Fig. 25 depicts the time history of the added-mass coefficients at the midpoint of the cylinder $CLa(z_{mid}, t)$. In particular, the added-mass coefficient jumps from a small value to a relatively large one when the reduced velocity is large enough. This large value is around 2.5, which is larger than the value one. This phenomenon is consistent with the observation that the VIV frequency at the lock-in region as shown in Fig. 19 is lower than the first order natural frequency estimated with added-mass coefficients of value one. In Fig. 24, we observe added-mass coefficients close to zero or negative value (green to blue color region) when reduced velocity is low. The negative value of added-mass coefficients has also been observed and discussed a number of times in the literature; e.g., Keulegan and Carpenter (1958), Vandiver (1993), Gopalkrishnan

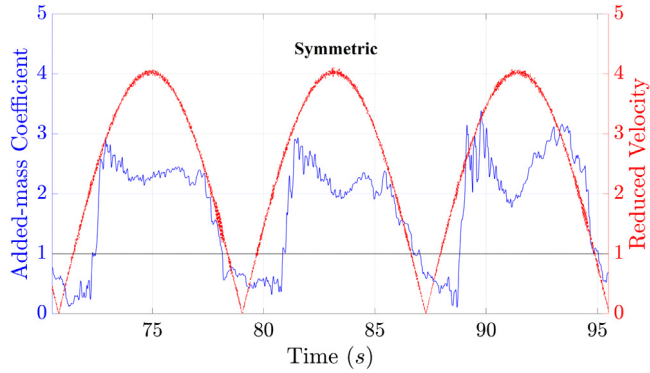


Fig. 25. The time history of the identified instantaneous added-mass coefficients at the midpoint of the cylinder $Cl(z_{mid}, t)$.

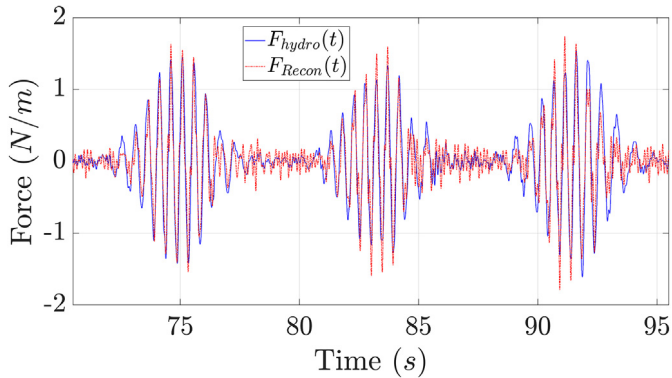


Fig. 26. A comparison between vortex-induced force at the mid point and the reconstructed force using the time-varying coefficient ($A_{osi} = 0.68$ m, $T_{osi} = 16.5$ s, $KC = 178$, $\max(V_r) = 4$).

(1993), Vikestad et al. (2000) and Sarpkaya (2010). The negative added-mass coefficients were also observed for a flexible cylinder under uniform flow (Song et al., 2016a), where the higher order mode responses are significant.

The identified instantaneous added-mass coefficient of the flexible cylinder under VIV is not equal to value '1' of an oscillating cylinder in ideal inviscid flow. Such a difference is also previously observed for a rigid cylinder under oscillatory flow at a large KC number (Sarpkaya, 1986), a forced oscillating cylinder (Gopalkrishnan, 1993), a free-vibrating rigid cylinder (Vikestad et al., 2000), and a flexible cylinder under uniform flow (Song et al., 2016a).

In Fig. 26, we compare the time history of the vortex-induced force at the midpoint of the cylinder and the reconstructed force using the time-varying coefficient at the midpoint of the cylinder. Results show that reconstructed force is able to reflect major characteristics of vortex-induced force. For low amplitude yet high frequency vibrations such as vibrations around $t = 80$ s, the reconstructed force overestimate hydrodynamic force. This indicates that Forgetting Factor Least Squares (FF-LS) method employed in this paper may be applicable within a certain frequency bandwidth, and we reserve detailed investigations of this method as a topic of ongoing work.

Furthermore, we look to compare the hydrodynamic coefficients identified here with a cylinder under modulated motion, which was documented in Chapter 5 of Gopalkrishnan (1993)'s thesis. The modulation motions of Gopalkrishnan (1993) are in the form of:

$$y(t) = Y_1 \sin(\omega_1 t) + Y_2 \sin(\omega_2 t) = 2Y_1 \cos\left(\frac{\omega_1 - \omega_2}{2}t\right) \sin\left(\frac{\omega_1 + \omega_2}{2}t\right) \quad (4.4a)$$

$$:= 2Y_1 \cos(2\pi f_m t) \sin(2\pi f_c t), \quad (4.4b)$$

where the amplitude modulation is expressed as the superposition of two distinct frequency sinusoidal motion with the same amplitude. For the flexible cylinder discussed here, the carrier frequency is approximately $f_c = 2$ Hz as identified from the wavelet analysis in Fig. 19, and the modulation frequency is estimated as the frequency of the relative oscillatory flow; i.e., $f_m = 1/T_{osi}$. Thus, according to equation (5.3) in Gopalkrishnan (1993), we have the modulation ratio $1:(f_c/2f_m)$ for the flexible cylinder at approximately 1:16.5. We extract the excitation and added-mass coefficients from Gopalkrishnan (1993) for both modulation ratios 1:10 and 1:20. We calculate the instantaneous non-dimensional frequency as $f^* = \frac{Df_c}{U(t)}$ to include the time-varying effects of a flexible cylinder under oscillatory flow. For coefficients with

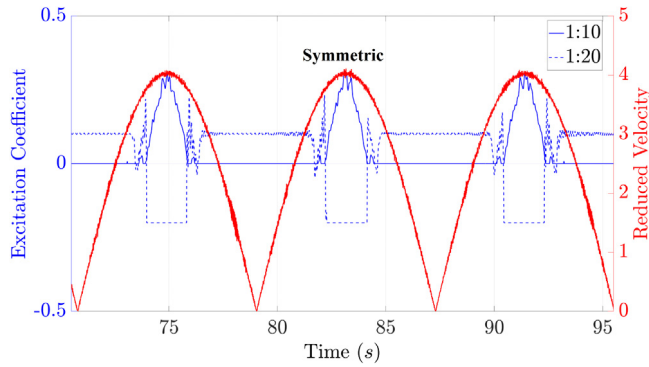


Fig. 27. The excitation coefficients for the midpoint of the cylinder obtained from Gopalkrishnan (1993) at modulation ratios 1:10 and 1:20, respectively.

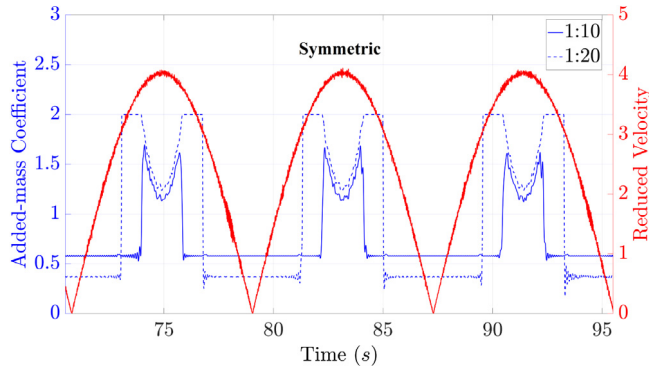


Fig. 28. The added-mass coefficients for the midpoint of the cylinder obtained from Gopalkrishnan (1993) at modulation ratios 1:10 and 1:20, respectively.

the peak amplitude ratio and non-dimensional frequency inside of the database of Gopalkrishnan (1993), we interpolate with a bilinear function to obtain the coefficients, and for coefficients with those parameters outside of the database of Gopalkrishnan (1993), we choose the closest value to get the coefficients. The excitation coefficients and the added-mass coefficients obtained from Gopalkrishnan (1993) are depicted in Figs. 27 and 28, respectively. The peak amplitudes for these results are chosen as the amplitude at the midpoint of the cylinder.

We find a qualitative difference that the identified excitation coefficients in Fig. 23 are not symmetric when the reduced velocity is symmetric through comparing the semi-empirical excitation coefficients in Fig. 27. At the ‘building-up’ region, the excitation coefficients are positive, while the excitation coefficients are negative at the ‘dying-out’ region of VIV. However, at the same reduced velocity and amplitude region, the traditional semi-empirical prediction method will result in the same excitation coefficients as the database is only related to these two parameters. The observation of identified excitation coefficients for both the flexible cylinder (Fig. 23) and the analytical modulated signal in Fig. 4 indicates that the excitation coefficients are also related to other parameters.

The temporal derivative of instantaneous amplitude $dA_{tot}(t)/dt$ is one of the determining parameters for the excitation coefficients, if we review the expression between the time-varying excitation coefficients $CLe(t)$ as well as the instantaneous amplitude $A_{tot}(t)$ and frequency $f_{tot}(t)$ in Eq. (3.9a). From Eq. (3.9a), we can see that the sign of $dA_{tot}(t)/dt$ determines the sign of the excitation coefficients if the structural damping is negligible as discussed before. However, this parameter $dA_{tot}(t)/dt$ is not considered in current hydrodynamics database, which leads to the qualitative difference from the identified excitation coefficients. To improve the qualitative property of excitation coefficients for predicting amplitude modulation, it is suggested including the temporal derivative of the amplitude $dA_{tot}(t)/dt$ to build the database of excitation coefficients.

If we assume the instantaneous amplitude is proportional to the reduced velocity, this suggests including the temporal derivative of the reduced velocity to build the database of excitation coefficients. Resvanis (2014) and Resvanis et al. (2015) also analyzed vortex-induced vibration of a flexible cylinder under ‘ramp test’ and they proposed a dimensionless parameter $\gamma = \frac{\partial U}{\partial t} T_n/U$, which represents the accelerating rate of the flow velocity. Under different accelerating rate of the flow velocity, the VIV responses show different characteristics, which further support to include the temporal derivative of the amplitude $dA_{tot}(t)/dt$ to build the database of excitation coefficients.

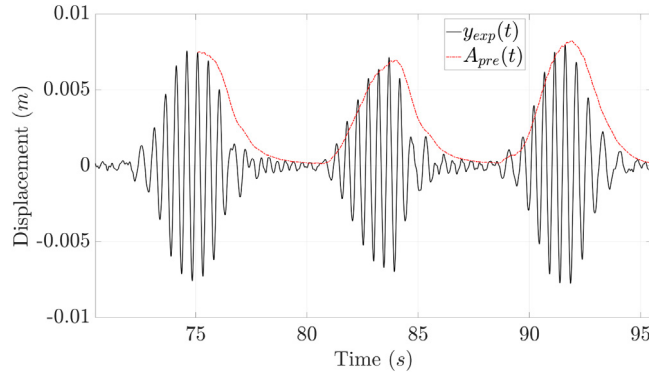


Fig. 29. A comparison between the experimental displacement $y_{exp}(t)$ at the midpoint of the cylinder and the predicted amplitude $A_{pre}(t)$ using time-varying hydrodynamics $CLe(z, t)$ and $CLa(z, t)$.

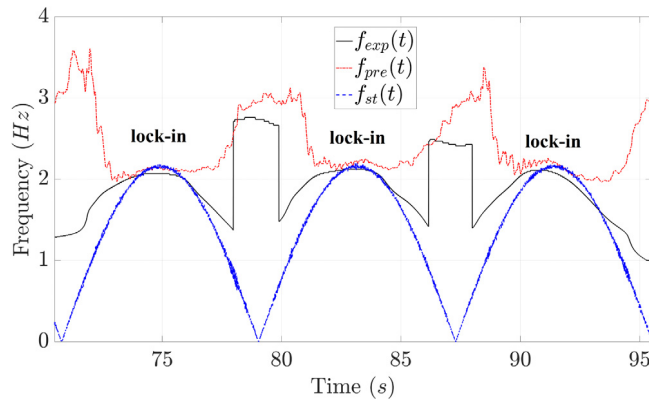


Fig. 30. A comparison among the instantaneous frequency of experimental VIV: $f_{exp}(t)$ obtained using wavelet analysis, the predicted instantaneous frequency $f_{pre}(t)$ using the time-varying hydrodynamics $CLe(z, t)$ and $CLa(z, t)$ and vortex shedding frequency $f_{st}(t)$ computed with $St = 0.2$.

For the added-mass coefficients, the identified ones indicate qualitative similarity to those obtained from the database of Gopalkrishnan (1993), but suggest quantitative improvements for the database. These added-mass coefficients both show symmetry when the reduced velocities are symmetric, which is consistent with the observation in Eq. (3.9b). This equation indicates that the added-mass coefficients are not related to the sign of $dA_{tot}(t)/dt$, but are only related to the magnitude of $dA_{tot}(t)/dt$, instantaneous amplitude $A_{tot}(t)$, and frequency $f_{tot}(t)$. However, current database does not include the effects of the temporal derivative of instantaneous amplitude $dA_{tot}(t)/dt$, which is likely to result in the quantitative difference from identified added-mass coefficients. Including the influence of $dA_{tot}(t)/dt$ offers the potential of quantitative improvement on the added-mass coefficients in the database.

4.4. The influence of the time-varying hydrodynamics on the modulated VIV

In this subsection, we discuss the effect of the time-varying hydrodynamics on modulated VIV. We initially use the time-varying hydrodynamic coefficients obtained in the previous subsection to predict the instantaneous amplitude and frequency according to the process in Section 3.3. Here, we use the corresponding parameters for this flexible cylinder as listed in Table 3. We only consider the first order instantaneous amplitude $A_{pre,1}(t)$ and frequency $f_{pre,1}(t)$, and they are denoted as $A_{pre}(t)$ and $f_{pre}(t)$ for the ease of exposition. Extending this prediction method for higher order response is one of ongoing work directions.

The identified time-varying hydrodynamic coefficients allow us to predict the amplitude and frequency modulation relatively close to experimental results. Fig. 29 predicts the instantaneous amplitude using obtained time-varying hydrodynamic coefficients, and results are close to the envelope of the VIV displacement observed from the experimental data. In Fig. 30, we compare the instantaneous frequency from the experimental data, that predicted from obtained time-varying hydrodynamic coefficients and vortex shedding frequency computed with Strouhal number $St = 0.2$: $f_{st}(t) = \frac{St|U(t)|}{D}$. This Strouhal number $St = 0.2$ is chosen according to the Reynolds number based on the maximum relative flow velocity $Re = \frac{\max|U(t)|D}{v} = 6220$ (Fu et al., 2014) and the relationship between the Strouhal number and

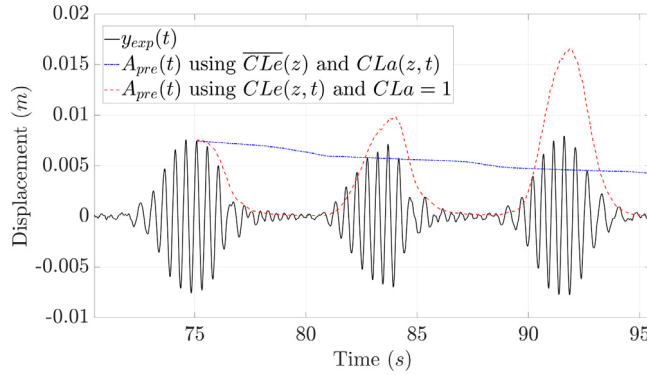


Fig. 31. A comparison among the experimental displacement $y_{exp}(t)$ at the midpoint of the cylinder, the instantaneous amplitude $A_{pre}(t)$ predicted using the time averaged excitation coefficients $\overline{CLe}(z)$ with the time-varying added-mass coefficients $CLa(z, t)$, and the instantaneous amplitude $A_{pre}(t)$ predicted using the time-varying excitation coefficients $CLe(z, t)$ with the constant added-mass coefficient $CLa = 1$.

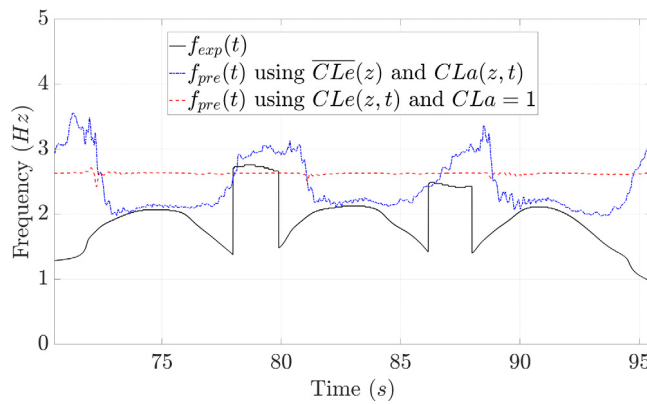


Fig. 32. A comparison among the instantaneous frequency of experimental VIV: $f_{exp}(t)$ obtained using wavelet analysis, the instantaneous frequency $f_{pre}(t)$ predicted using the time averaged excitation coefficients $\overline{CLe}(z)$ with the time-varying added-mass coefficients $CLa(z, t)$, and the instantaneous frequency $f_{pre}(t)$ predicted using the time-varying excitation coefficients $CLe(z, t)$ with the constant added-mass coefficient $CLa = 1$.

the Reynolds number; e.g., figure 3.3 of [Blevins \(1977\)](#). Results show that the time-varying hydrodynamics allows us to predict the frequency modulation VIV (time-sharing effects). At the ‘lock-in’ of VIV, the predicted vibration frequency is close to experimental data and the vortex shedding frequency computed with $St = 0.2$. This indicates that the variation of the added-mass coefficients makes the vibration frequency close to the vortex-shedding frequency, and therefore, lock-in of VIV occurs.

Moreover, we replace parts of the time-varying hydrodynamic coefficients as time-invariant ones to reveal the effects of time-varying hydrodynamics. In one case, we replace the time-varying excitation coefficients $CLe(z, t)$ as its time-averaged value: $\overline{CLe}(z)$, and in another case, we replace the time-varying added-mass coefficients $CLa(z, t)$ as the constant added-mass coefficient $CLa = 1$, which is the added-mass coefficient of a rigid cylinder in ideal inviscid flow.

The time-varying excitation coefficients are critical for amplitude modulation prediction. In Fig. 31, we compare the experimental displacement $y_{exp}(t)$ at the midpoint of the cylinder, the instantaneous amplitude $A_{pre}(t)$ predicted using the time averaged excitation coefficients $\overline{CLe}(z)$ with time-varying added-mass coefficients $CLa(z, t)$, and the instantaneous amplitude $A_{pre}(t)$ predicted using the time-varying excitation coefficients $CLe(z, t)$ with constant added-mass coefficient $CLa = 1$. If we use the time-averaged excitation coefficient, the predicted vibration will exponentially decay/grow instead of showing amplitude modulation phenomenon. Also, results indicate that the time-varying added-mass coefficients are also essential to predict the accurate amplitude modulation. These effects are similar to the analysis of Fig. 10 in Section 3.2.

On the prediction of instantaneous frequency, treating excitation coefficients as the time-averaged value do not have much influence, but the added-mass is more important. Fig. 32 compares the instantaneous frequency of the experimental VIV: $f_{exp}(t)$ obtained using wavelet analysis, the instantaneous frequency $f_{pre}(t)$ predicted using the time averaged excitation coefficients $\overline{CLe}(z)$ with the time-varying added-mass coefficients $CLa(z, t)$, and the instantaneous frequency $f_{pre}(t)$ predicted using the time-varying excitation coefficients $CLe(z, t)$ with the constant added-mass coefficient $CLa = 1$. The predicted instantaneous frequency is close to the original prediction results in Fig. 30 although we replace

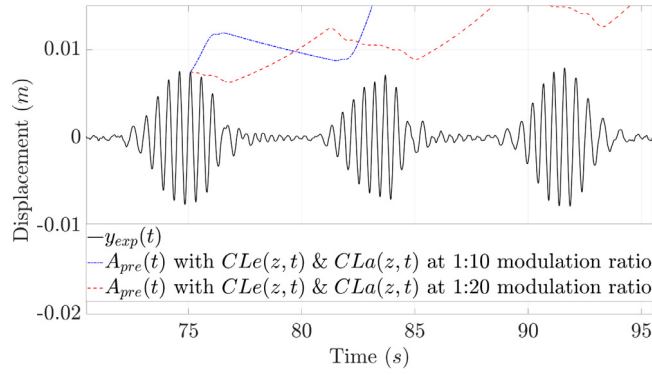


Fig. 33. A comparison among the experimental displacement $y_{exp}(t)$ at the midpoint of the cylinder, the instantaneous amplitude $A_{pre}(t)$ predicted using the coefficients $CLe(z, t)$, $CLa(z, t)$ obtained from Gopalkrishnan (1993) at modulation ratio 1:10 and 1:20, respectively.

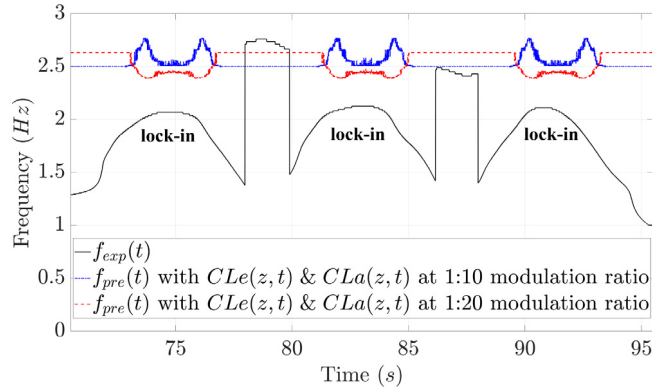


Fig. 34. A comparison among the instantaneous frequency of experimental VIV: $f_{exp}(t)$ obtained using wavelet analysis, the instantaneous frequency $f_{pre}(t)$ predicted using the coefficients $CLe(z, t)$, $CLa(z, t)$ obtained from Gopalkrishnan (1993) at modulation ratio 1:10 and 1:20, respectively.

time-varying excitation coefficients as the time-averaged value. However, if we use the constant added-mass coefficients $CLa = 1$ instead of the time-varying added-mass coefficients $CLa(z, t)$, we cannot predict the frequency modulation effect and actually, the predicted vibration frequency is not close to the experimental VIV frequency. These effects are similar to the analysis of Fig. 11 in Section 3.2.

Furthermore, we predict the instantaneous amplitude and frequency using the coefficients obtained from the database of Gopalkrishnan (1993) as described in the previous subsection. Here, the peak amplitude varies for each axial location of the cylinder $y_{max}(z) = \max_t y(z, t)$, which allows us to obtain the spatial-temporal varying coefficients from the database.

It is essential to include the influence of the derivative of instantaneous amplitude $dA_{tot}(t)/dt$ on excitation coefficients in the database. Fig. 33 compares the experimental displacement $y_{exp}(t)$ with the instantaneous amplitude $A_{pre}(t)$ predicted using the coefficients from Gopalkrishnan (1993), and the predicted amplitude $A_{pre}(t)$ cannot reflect the amplitude modulation effect of the flexible cylinder. This results from the fact that the present hydrodynamic coefficients database does not include the influence of the derivative of instantaneous amplitude $dA_{tot}(t)/dt$ on excitation coefficients, which leads to the symmetric excitation coefficients when the reduced velocity is symmetric as shown in Fig. 27. According to the connection between the excitation coefficients and the amplitude modulation demonstrated in Figs. 10 and 31 as well as Eq. (3.9a), it is suggested including the influence of the derivative of the instantaneous amplitude $dA_{tot}(t)/dt$ to capture the amplitude modulation of VIV; i.e., the VIV ‘building-up’, ‘lock-in’, and ‘dying out’ processes.

Quantitative improvement for the added-mass database is critical to predict the frequency of modulated VIV under oscillatory flow. In Fig. 34, the instantaneous frequency is predicted using the added-mass coefficients from the database of Gopalkrishnan (1993), and these results deviates from the VIV frequency observed in experiments. As indicated in Eq. (3.9b), the derivative of instantaneous amplitude $dA_{tot}(t)/dt$ also plays a role in the added-mass coefficients. It is advised to consider the influence of $dA_{tot}(t)/dt$ to improve the added-mass coefficients quantitatively.

5. Concluding remarks

This paper employs the Forgetting Factor Least Squares (FF-LS) method for the identification of time-varying hydrodynamics of a flexible cylinder under modulated vortex-induced vibrations (VIV). Different from the least squares

method used for identification of hydrodynamics, where equal weights are put on all sampled data, this method introduces a forgetting factor to provide a greater weight to the data closer to the present moment. This leads to the possibility of dealing with the time-varying parameters. The FF-LS method's applicability to accurately identify time-varying hydrodynamic coefficients is firstly demonstrated through an elastically mounted rigid cylinder under flow with given synthesized modulated motion. Results show that time-varying hydrodynamic coefficients allow us to accurately reconstruct the hydrodynamic force acting on a cylinder under modulated motion, while constant coefficients identified by least squares method fail.

In order to analyze the influence of time-varying hydrodynamic coefficients on VIV response, we propose the framework to predict the instantaneous amplitude and frequency using time-varying hydrodynamic coefficients. This method computes the time-varying eigenvalues at each time step. The real part of the eigenvalue includes the information of amplitude modulation, and the imaginary part of the eigenvalue represents the frequency modulation. The effects of time-varying coefficients on predicting the modulated VIV are analyzed numerically, and the analytical expressions between time-varying hydrodynamic coefficients and the modulated VIV are established. Both numerical and analytical results reveal the physics insight of time-varying hydrodynamic coefficients and the hydrodynamic mechanism behind the modulated VIV; i.e., the time-varying excitation coefficients mainly influence the amplitude modulation, and the time-varying added-mass coefficients contain the major information of frequency modulation. The results further suggest to include the influence of temporal derivative of instantaneous amplitude $dA_{tot}(t)/dt$ on hydrodynamic coefficients. This prediction method is also extended to a highly tensioned flexible cylinder through Fourier series expansion and the Galerkin method in spatial domain.

By performing the identification procedure for all the sampled data of a flexible cylinder undergoing the modulated VIV, the corresponding time-varying hydrodynamics in the cross-flow direction considering the amplitude modulation and frequency modulation are obtained. The results show that, under modulated VIV, hydrodynamic coefficients of the flexible cylinder also show time-varying characteristics. The excitation coefficients reveal a qualitative difference from those obtained from the database of a cylinder with modulated motion under flow. This difference and theoretical analysis suggest considering the influence of the temporal derivative of instantaneous amplitude dA_{tot}/dt on excitation coefficients in the database to improve the prediction of amplitude modulation. The added-mass coefficients show qualitative similarity to those obtained from the database of a cylinder, but they are quantitatively different.

We further use the obtained time-varying hydrodynamic coefficients to predict the instantaneous amplitude and frequency of a flexible cylinder under VIV. Results reveal that using time-varying excitation coefficients and added-mass coefficients together, the predicted instantaneous amplitude and frequency are close to the experimental results. When replacing the time-varying excitation coefficients as the time-averaged value, the predicted amplitude only show exponential decay/grow instead of modulation. When replacing the time-varying added-mass coefficients as the added-mass coefficient in still water $C_L = 1$, the predicted frequency does not show modulation effects and is not close to VIV frequency in experiments. When using the coefficients obtained from the database of a cylinder with modulated motion under flow, the prediction results further suggests the necessity to consider the influence of the temporal derivative of instantaneous amplitude dA_{tot}/dt to improve the excitation coefficients qualitatively and the added-mass coefficients quantitatively and thus to improve the prediction of modulated VIV.

The results presented here could be extended in a number of ways. Initially, it would be meaningful to consider the influence of the temporal derivative of instantaneous amplitude dA_{tot}/dt and re-analyze current available hydrodynamic database of modulated VIV or multi-frequency VIV (Gopalkrishnan, 1993; Dahl et al., 2007; Aronsen, 2007; Aronsen and Larsen, 2007; Swithenbank, 2007; Fu et al., 2014; Resvanis, 2014; Resvanis et al., 2015). Building a more comprehensive database that includes the influence of dA_{tot}/dt will be promising for the modulated VIV prediction. At last, the modulation prediction approach here for the flexible cylinder described in Section 3.3 and Appendix B only considers the first mode. Extending the modulation prediction method to the higher mode VIV and to consider the interaction between different modes will be interesting.

Declaration of competing interest

The authors declare that they have no known competing financial interests or personal relationships that could have appeared to influence the work reported in this paper.

Acknowledgments

This research was supported by the National Science Fund for Distinguished Young Scholars of China under Grant Number 51825903, the Joint Funds of the National Natural Science Foundation of China under Grant Number U19B2013 and the 13th Five-Year Plan National Science and Technology Major Project of China under Grant number 2016ZX05028-001.

Appendix A. The recursive form of the forgetting factor least squares method

Following Eq. (2.14), we derive the recursive version of the forgetting-factor least squares method; i.e., the *Forgetting Factor Recursive Least Squares* (FF-RLS) method. Defining:

$$\mathbf{P}^{-1}(k) := \sum_{i=1}^k \mu^{k-i} \mathbf{h}(i) \mathbf{h}^T(i) = \hat{\mathbf{H}}_k^T \hat{\mathbf{H}}_k, \quad (\text{A.1a})$$

$$\mathbf{P}^{-1}(k-1) := \sum_{i=1}^{k-1} \mu^{k-1-i} \mathbf{h}(i) \mathbf{h}^T(i) = \hat{\mathbf{H}}_{k-1}^T \hat{\mathbf{H}}_{k-1}, \quad (\text{A.1b})$$

$$\hat{\mathbf{H}}_{k-1} := \begin{bmatrix} \beta^{k-2} \mathbf{h}^T(1) \\ \beta^{k-3} \mathbf{h}^T(2) \\ \vdots \\ \beta \mathbf{h}^T(k-2) \\ \mathbf{h}^T(k-1) \end{bmatrix}, \quad \hat{\mathbf{H}}_k := \begin{bmatrix} \beta \hat{\mathbf{H}}_{k-1} \\ \mathbf{h}^T(k) \end{bmatrix}, \quad (\text{A.1c})$$

then we have:

$$\mathbf{P}^{-1}(k) = \sum_{i=1}^{k-1} \mu^{k-1-i} \mathbf{h}^T(i) \mathbf{h}^T(i) + \mathbf{h}(k) \mathbf{h}^T(k) = \mu \mathbf{P}^{-1}(k-1) + \mathbf{h}(k) \mathbf{h}^T(k). \quad (\text{A.2})$$

Setting:

$$\hat{\mathbf{f}}_{k-1} = [\beta^{k-2} f_{CF}(1) \quad \beta^{k-3} f_{CF}(2) \quad \cdots \quad \beta f_{CF}(k-2) \quad f_{CF}(k-1)]^T, \quad \text{and} \quad (\text{A.3a})$$

$$\hat{\mathbf{f}}_k = \begin{bmatrix} \beta \hat{\mathbf{f}}_{k-1} \\ f_{CF}(k) \end{bmatrix}, \quad (\text{A.3b})$$

then we have:

$$\hat{\theta}(k-1) = (\hat{\mathbf{H}}_{k-1}^T \hat{\mathbf{H}}_{k-1})^{-1} \hat{\mathbf{H}}_{k-1}^T \hat{\mathbf{f}}_{k-1} \quad (\text{A.4a})$$

$$= \mathbf{P}(k-1) \left[\sum_{i=1}^{k-1} \mu^{k-1-i} \mathbf{h}(i) f_{CF}(i) \right], \quad (\text{A.4b})$$

or

$$\mathbf{P}^{-1}(k-1) \hat{\theta}(k-1) = \sum_{i=1}^{k-1} \mu^{k-1-i} \mathbf{h}(i) f_{CF}(i). \quad (\text{A.5})$$

Using Eqs. (A.2) and (A.5), we have:

$$\hat{\theta}(k) = (\hat{\mathbf{H}}_k^T \hat{\mathbf{H}}_k)^{-1} \hat{\mathbf{H}}_k^T \hat{\mathbf{f}}_k = \mathbf{P}(k) \left[\sum_{i=1}^k \mu^{k-i} \mathbf{h}(i) f_{CF}(i) \right] \quad (\text{A.6a})$$

$$= \mathbf{P}(k) [\mu \mathbf{P}^{-1}(k-1) \hat{\theta}(k-1) + \mathbf{h}(k) f_{CF}(k)] \quad (\text{A.6b})$$

$$= \hat{\theta}(k-1) + \mathbf{P}(k) \mathbf{h}(k) [f_{CF}(k) - \mathbf{h}^T(k) \hat{\theta}(k-1)]. \quad (\text{A.6c})$$

Setting the gain matrix as:

$$\mathbf{K}(k) := \mathbf{P}(k) \mathbf{h}(k), \quad (\text{A.7})$$

then Eq. (A.6c) can be written as:

$$\hat{\theta}(k) = \hat{\theta}(k-1) + \mathbf{K}(k) [f_{CF}(k) - \mathbf{h}^T(k) \hat{\theta}(k-1)]. \quad (\text{A.8a})$$

Furthermore, we use the matrix inverse lemma or Sherman–Morrison–Woodbury formula; see e.g., Hager (1989):

$$(\mathbf{A} + \mathbf{B}\mathbf{C})^{-1} = \mathbf{A}^{-1} - \mathbf{A}^{-1}\mathbf{B}(\mathbf{I} + \mathbf{C}\mathbf{A}^{-1}\mathbf{B})^{-1}\mathbf{C}\mathbf{A}^{-1} \quad (\text{A.9})$$

to rewrite Eq. (A.2) as:

$$\mathbf{P}(k) = [\mu \mathbf{P}^{-1}(k-1) + \mathbf{h}(k) \mathbf{h}^T(k)]^{-1} \quad (\text{A.10})$$

$$= \frac{1}{\mu} [\mathbf{I} - \frac{\mathbf{P}(k-1) \mathbf{h}(k) \mathbf{h}^T(k)}{\mathbf{h}^T(k) \mathbf{P}(k-1) \mathbf{h}(k) + \mu}] \mathbf{P}(k-1). \quad (\text{A.11})$$

Substituting the above equation into Eq. (A.7), we have:

$$\mathbf{K}(k) = \mathbf{P}(k-1)\mathbf{h}(k)[\mathbf{h}^T(k)\mathbf{P}(k-1)\mathbf{h}(k) + \mu]^{-1}. \quad (\text{A.12})$$

We can further use Eq. (A.12) to simplify Eq. (A.11) as:

$$\mathbf{P}(k) = \frac{1}{\mu}[\mathbf{I} - \mathbf{K}(k)\mathbf{h}^T(k)]\mathbf{P}(k-1). \quad (\text{A.13})$$

In summary, the Forgetting Factor Recursive Least Squares method can be written as:

$$\mathbf{K}(k) = \mathbf{P}(k-1)\mathbf{h}(k)[\mathbf{h}^T(k)\mathbf{P}(k-1)\mathbf{h}(k) + \mu]^{-1}, \quad (\text{A.14a})$$

$$\mathbf{P}(k) = \frac{1}{\mu}[\mathbf{I} - \mathbf{K}(k)\mathbf{h}^T(k)]\mathbf{P}(k-1), \quad (\text{A.14b})$$

$$\hat{\theta}(k) = \hat{\theta}(k-1) + \mathbf{K}(k)[f_{CF}(k) - \mathbf{h}^T(k)\hat{\theta}(k-1)], \quad (\text{A.14c})$$

$$0 < \mu \leq 1. \quad (\text{A.14d})$$

To start this recursive algorithm, we need to set up the initial estimation of $\hat{\theta}(1)$ and $\mathbf{P}(1)$. These initial value settings do not influence the estimated time-varying coefficients in the following periods. For results in Section 2.2, we set $CLe(t_1) = 0.293$ and $CLa(t_1) = -1.151$ as the $\hat{\theta}(1)$ and set $\mathbf{P}(1)$ as an identity matrix.

Appendix B. The Galerkin method for predicting modulation of a flexible cylinder

Substituting Eq. (3.14) back into the governing equation of the flexible cylinder in Eq. (3.12), it gives:

$$\begin{aligned} & [m + \frac{\rho\pi D^2}{4} CLa(z, t)] \sum_{k=1}^n \frac{\partial^2 \hat{y}_k(t)}{\partial t^2} \sin(k \frac{z\pi}{L}) \\ & + [c - \frac{\rho DU_{RMS}^2(z, t)}{2v_0(z)} CLe(z, t)] \sum_{k=1}^n \frac{\partial \hat{y}_k(t)}{\partial t} \sin(k \frac{z\pi}{L}) \\ & + [EI \sum_{k=1}^n (k \frac{\pi}{L})^4 \hat{y}_k(t) \sin(k \frac{z\pi}{L})] + F_T(z, t) \sum_{k=1}^n (k \frac{\pi}{L})^2 \hat{y}_k(t) \sin(k \frac{z\pi}{L}) = 0. \end{aligned} \quad (\text{B.1})$$

Then, the Galerkin method requires that the residue of Eq. (B.1) is orthogonal to a set of test function, which is the same as the basis functions; i.e., $\sin(j \frac{z\pi}{L})$, $j = 1, 2, 3, \dots, n$. We multiply Eq. (B.1) with $\sin(j \frac{z\pi}{L})$ and integrate over z from 0 to L :

$$\begin{aligned} & \sum_{k=1}^n \left\{ \int_0^L [m + \frac{\rho\pi D^2}{4} CLa(z, t)] \sin(k \frac{z\pi}{L}) \sin(j \frac{z\pi}{L}) dz \right\} \frac{\partial^2 \hat{y}_k(t)}{\partial t^2} \\ & + \sum_{k=1}^n \left\{ \int_0^L [c - \frac{\rho DU_{RMS}^2(z, t)}{2v_0(z)} CLe(z, t)] \sin(k \frac{z\pi}{L}) \sin(j \frac{z\pi}{L}) dz \right\} \frac{\partial \hat{y}_k(t)}{\partial t} \\ & + \sum_{k=1}^n \left\{ \int_0^L [EI(k \frac{\pi}{L})^4 + F_T(z, t)(k \frac{\pi}{L})^2] \sin(k \frac{z\pi}{L}) \sin(j \frac{z\pi}{L}) dz \right\} \hat{y}_k(t) = 0, \quad j = 1, 2, 3, \dots, n. \end{aligned} \quad (\text{B.2})$$

Then, we define the matrix with its elements:

$$[\hat{\mathbf{M}}]_{j,k}(t) = \int_0^L [m + \frac{\rho\pi D^2}{4} CLa(z, t)] \sin(k \frac{z\pi}{L}) \sin(j \frac{z\pi}{L}) dz, \quad (\text{B.3a})$$

$$[\hat{\mathbf{C}}]_{j,k}(t) = \int_0^L [c - \frac{\rho DU_{RMS}^2(z, t)}{2v_0(z)} CLe(z, t)] \sin(k \frac{z\pi}{L}) \sin(j \frac{z\pi}{L}) dz, \quad (\text{B.3b})$$

$$[\hat{\mathbf{K}}]_{j,k}(t) = \int_0^L [EI(k \frac{\pi}{L})^4 + F_T(z, t)(k \frac{\pi}{L})^2] \sin(k \frac{z\pi}{L}) \sin(j \frac{z\pi}{L}) dz, \quad j, k = 1, 2, \dots, n, \quad (\text{B.3c})$$

and we can obtain the expression as Eq. (3.16):

$$\hat{\mathbf{M}}(t) \frac{\partial^2}{\partial t^2} \hat{\mathbf{y}}(t) + \hat{\mathbf{C}}(t) \frac{\partial}{\partial t} \hat{\mathbf{y}}(t) + \hat{\mathbf{K}}(t) \hat{\mathbf{y}}(t) = \mathbf{0}. \quad (\text{B.4})$$

Note that when the hydrodynamic coefficients and tension are invariant over the spatial variable z , or the cylinder location, we hold that $\hat{\mathbf{M}}$, $\hat{\mathbf{C}}$, and $\hat{\mathbf{K}}$ become the diagonal matrices, considering the orthogonality of the sinusoidal function; i.e.,

$$\int_0^L \sin(k \frac{z\pi}{L}) \sin(j \frac{z\pi}{L}) dz = \begin{cases} L/2, & k=j \\ 0, & k \neq j. \end{cases} \quad (\text{B.5})$$

In this case, the motion at all basis functions $\sin(k \frac{z\pi}{L})$, $k = 1, 2, \dots, n$ (sinusoidal mode) are uncoupled, and thus we can treat the flexible cylinder as several uncoupled mass-spring-dashpot system. In this sense, the discussions on the effect of time-varying hydrodynamics in Sections 3.2 and 3.3 also hold. However, we also note that typically hydrodynamic coefficients also vary over spatial variable z (Song et al., 2016a), and it is shown that additional concepts are required to build a mapping between a flexible cylinder and rigid one under uniform flow (Fan et al., 2019). At last, this prediction method for the flexible cylinder also shows some similarity to the modal space prediction method (Lu et al., 2018, 2019).

Appendix C. Bending strain and bending displacement

The axial tension of the cylinder model will change periodically when the cylinder undergoes vortex-induced vibration. The strain $\epsilon_{CF,a}(z, t)$ and $\epsilon_{CF,c}(z, t)$ measured by the FBG strain sensor in the CF direction will include two parts: tensile strain caused by axial tension $\epsilon_{CF,T}(z, t)$ and bending strain $\epsilon_{CF}(z, t)$ generated by VIV:

$$\epsilon_{CF,a}(z, t) = \epsilon_{CF,T}(z, t) + \epsilon_{CF}(z, t), \text{ and} \quad (\text{C.1a})$$

$$\epsilon_{CF,c}(z, t) = \epsilon_{CF,T}(z, t) - \epsilon_{CF}(z, t). \quad (\text{C.1b})$$

Transforming the above equation, then bending strain $\epsilon_{CF}(z, t)$ in the CF direction caused by VIV is:

$$\epsilon_{CF}(z, t) = [\epsilon_{CF,a}(z, t) - \epsilon_{CF,c}(z, t)]/2, \quad (\text{C.2})$$

When the bending strain of the cylinder is obtained, the bending displacement of the cylinder can be obtained by modal analysis. For example, the time history of VIV displacement $y(z, t)$ in the CF direction of the cylinder at node z can be expressed as:

$$y(z, t) = \sum_{i=h}^k p_i(t) \phi_i(z), \quad z \in [0, L], \quad (\text{C.3})$$

where $\phi_i(z)$ is the i^{th} displacement mode of the cylinder in the local coordinate system, and $p_i(t)$ is the time history of the displacement weight.

The bending displacement $y(z, t)$ in the CF direction and bending strain $\epsilon_{CF}(z, t)$ satisfy the equation below:

$$\frac{\partial^2 y(z, t)}{\partial z^2} = -\frac{\epsilon_{CF}(z, t)}{R}. \quad (\text{C.4})$$

From Eqs. (C.3) and (C.4), the bending strain $\epsilon(z, t)$ can be obtained:

$$\epsilon_{CF}(z, t) = -R \sum_{i=h}^k p_i(t) \frac{\partial^2 \phi_i(z)}{\partial z^2}. \quad (\text{C.5})$$

Therefore, when the bending strain of the cylinder in the CF direction is obtained from Eq. (C.2), the time history of the displacement mode weight $p_i(t)$ can be obtained according to Eq. (C.5). Then the bending displacement response $y(z, t)$ of the cylinder in the CF direction can be obtained by Eq. (C.3).

References

- Akhtar, I., Marzouk, O.A., Nayfeh, A.H., 2009. A van der Pol-Duffing oscillator model of hydrodynamic forces on canonical structures. *J. Comput. Nonlinear Dyn.* 4 (4).
- Alfossail, F.K., Younis, M.I., 2019a. Multifrequency excitation of an inclined marine riser under internal resonances. *Nonlinear Dyn.* 1–23.
- Alfossail, F.K., Younis, M.I., 2019b. Two-to-one internal resonance of an inclined marine riser under harmonic excitations. *Nonlinear Dyn.* 95 (2), 1301–1321.
- Allen, J., 1977. Short term spectral analysis, synthesis, and modification by discrete Fourier transform. *IEEE Trans. Acoust. Speech Signal Process.* 25 (3), 235–238.
- Aronsen, K.H., 2007. An Experimental Investigation of In-Line and Combined In-Line and Cross-Flow Vortex Induced Vibrations (Ph.D. thesis). Norwegian University of Science and Technology.
- Aronsen, K.H., Larsen, C.M., 2007. Hydrodynamic coefficients for in-line vortex induced vibrations. In: ASME 2007 26th International Conference on Ocean, Offshore and Arctic Engineering, pp. 949–956.
- Bender, C.M., Orszag, S.A., 2013. Advanced Mathematical Methods for Scientists and Engineers I: Asymptotic Methods and Perturbation Theory. Springer Science & Business Media.
- Blevins, R.D., 1977. Flow-Induced Vibration. Van Nostrand Reinhold Co., New York, p. 377.
- Boashash, B., 2016. Chapter I: The time-frequency approach: Essence and terminology. In: Time-Frequency Signal Analysis and Processing, second ed. Academic Press, pp. 3–29.

- Bourguet, R., Karniadakis, G.E., Triantafyllou, M.S., 2011. Vortex-induced vibrations of a long flexible cylinder in shear flow. *J. Fluid Mech.* 677, 342–382.
- Bourguet, R., Karniadakis, G.E., Triantafyllou, M.S., 2013. Distributed lock-in drives broadband vortex-induced vibrations of a long flexible cylinder in shear flow. *J. Fluid Mech.* 717, 361–375.
- Brika, D., Laneville, A., 1993. Vortex-induced vibrations of a long flexible circular cylinder. *J. Fluid Mech.* 250, 481–508.
- Brunton, S.L., Proctor, J.L., Kutz, J.N., 2016. Discovering governing equations from data by sparse identification of nonlinear dynamical systems. *Proc. Natl. Acad. Sci.* 113 (15), 3932–3937.
- Champion, K.P., Brunton, S.L., Kutz, J.N., 2019. Discovery of nonlinear multiscale systems: Sampling strategies and embeddings. *SIAM J. Appl. Dyn. Syst.* 18 (1), 312–333.
- Chang, S.H.M., Isherwood, M., 2003. Vortex-induced vibrations of steel catenary risers and steel offloading lines due to platform heave motions. In: Offshore Technology Conference.
- Chaplin, J.R., Bearman, P.W., Cheng, Y., Fontaine, E., Graham, J.M.R., Herfjord, K., Huera-Huarte, F.J., Isherwood, M., Lambrakos, K., Larsen, C.M., Meneghini, J.R., Moe, G., Pattenden, R.J., Triantafyllou, M.S., Willden, R.H.J., 2005a. Blind predictions of laboratory measurements of vortex-induced vibrations of a tension riser. *J. Fluids Struct.* 21 (1), 25–40.
- Chaplin, J.R., Bearman, P.W., Huera-Huarte, F.J., Pattenden, R.J., 2005b. Laboratory measurements of vortex-induced vibrations of a vertical tension riser in a stepped current. *J. Fluids Struct.* 21 (1), 3–24.
- Chavent, G., 1979. Identification of distributed parameter systems: about the output least square method, its implementation, and identifiability. *IFAC Proc. Vol.* 12 (8), 85–97.
- Chen, W., Li, M., Guo, S., Gan, K., 2014. Dynamic analysis of coupling between floating top-end heave and riser's vortex-induced vibration by using finite element simulations. *Appl. Ocean Res.* 48, 1–9.
- Cleveland, W.S., Devlin, S.J., 1988. Locally weighted regression: an approach to regression analysis by local fitting. *J. Am. Stat. Assoc.* 83 (403), 596–610.
- Dahl, J.M., Hover, F.S., Triantafyllou, M.S., Dong, S., Karniadakis, G.E., 2007. Resonant vibrations of bluff bodies cause multivortex shedding and high frequency forces. *Phys. Rev. Lett.* 99 (14), 144503.
- Ding, F., Chen, T., 2005. Performance bounds of forgetting factor least-squares algorithms for time-varying systems with finite measurement data. *IEEE Trans. Circuits Syst.* 52 (3), 555–566.
- Draper, N.R., 1984. The Box-Wetz criterion versus R^2 . *J. R. Stat. Soc. Ser. A* 147 (1), 100–103.
- Evangelinos, C., Karniadakis, G.E., 1999. Dynamics and flow structures in the turbulent wake of rigid and flexible cylinders subject to vortex-induced vibrations. *J. Fluid Mech.* 400, 91–124.
- Facchinetto, M.L., de Langre, E., Biolley, F., 2004. Coupling of structure and wake oscillators in vortex-induced vibrations. *J. Fluids Struct.* 19 (2), 123–140.
- Fan, D., Wang, Z., Triantafyllou, M.S., Karniadakis, G.E., 2019. Mapping the properties of the vortex-induced vibrations of flexible cylinders in uniform oncoming flow. *J. Fluid Mech.* 881, 815–858.
- Franzini, G.R., Gonçalves, R.T., Pesce, C.P., Fujarra, A.L.C., Mazzilli, C.E.N., Meneghini, J.R., Mendes, P., 2015a. Vortex-induced vibration experiments with a long semi-immersed flexible cylinder under tension modulation: Fourier transform and Hilbert–Huang spectral analyses. *J. Braz. Soc. Mech. Sci. Eng.* 37 (2), 589–599.
- Franzini, G.R., Pereira, A.A.P., Fujarra, A., Pesce, C.P., 2009. Experiments on VIV under frequency modulation and at constant Reynolds numbers. In: ASME 2008 27th International Conference on Offshore Mechanics and Arctic Engineering. pp. 959–968.
- Franzini, G.R., Pesce, C.P., Gonçalves, R.T., Fujarra, A.L.C., Mendes, P., 2018. An experimental investigation on concomitant vortex-induced vibration and axial top-motion excitation with a long flexible cylinder in vertical configuration. *Ocean Eng.* 156, 596–612.
- Franzini, G.R., Pesce, C.P., Gonçalves, R.T., Fujarra, A.L.C., Meneghini, J.R., 2010. An experimental investigation on frequency modulated VIV in a water channel. In: BBVIV6—Proceedings of the 6th Bluff Bodies Wakes and Vortex-Induced Vibrations Conference.
- Franzini, G.R., Pesce, C.P., Salles, R., Gonçalves, R.T., Fujarra, A.L.C., Mendes, P., 2015b. Experimental analysis of a vertical and flexible cylinder in water: response to top motion excitation and parametric resonance. *J. Vib. Acoust.* 137 (3), 031010.
- Fu, S., Wang, J., Baarholm, R., Wu, J., Larsen, C.M., 2013. VIV of flexible cylinder in oscillatory flow. In: ASME 2013 32th International Conference on Ocean, Offshore and Arctic Engineering. V007T08A021.
- Fu, S., Wang, J., Baarholm, R., Wu, J., Larsen, C.M., 2014. Features of vortex-induced vibration in oscillatory flow. *J. Offshore Mech. Arct. Eng.* 136 (1), 011801.
- Gonzalez, E.C., 2001. High Frequency Dynamic Response of Marine Risers with Application to Flow-Induced Vibration (Ph.D. thesis). Massachusetts Institute of Technology.
- Gopalkrishnan, R., 1993. Vortex-Induced Forces on Oscillating Bluff Cylinders (Ph.D. thesis). Woods Hole Oceanographic Institution MA.
- Govardhan, R., Williamson, C.H.K., 2000. Modes of vortex formation and frequency response of a freely vibrating cylinder. *J. Fluid Mech.* 420, 85–130.
- Grant, R.G., Litton, R.W., Mamidipudi, P., 1999. Highly compliant rigid (HCR) riser model tests and analysis. In: Offshore Technology Conference.
- Hager, W.W., 1989. Updating the inverse of a matrix. *SIAM Rev.* 31 (2), 221–239.
- Hover, F.S., Miller, S.N., Triantafyllou, M.S., 1997. Vortex-induced vibration of marine cables: experiments using force feedback. *J. Fluids Struct.* 11 (3), 307–326.
- Hover, F.S., Techet, A.H., Triantafyllou, M.S., 1998. Forces on oscillating uniform and tapered cylinders in cross flow. *J. Fluid Mech.* 363, 97–114.
- Huera-Huarte, F.J., Bearman, P.W., 2009a. Wake structures and vortex-induced vibrations of a long flexible cylinder—part 1: dynamic response. *J. Fluids Struct.* 25 (6), 969–990.
- Huera-Huarte, F.J., Bearman, P.W., 2009b. Wake structures and vortex-induced vibrations of a long flexible cylinder—part 2: drag coefficients and vortex modes. *J. Fluids Struct.* 25 (6), 991–1006.
- Huera-Huarte, F.J., Bearman, P.W., Chaplin, J.R., 2006. On the force distribution along the axis of a flexible circular cylinder undergoing multi-mode vortex-induced vibrations. *J. Fluids Struct.* 22 (6–7), 897–903.
- Ilyas, S., Alfossail, F.K., Younis, M.I., 2019. On the application of the multiple scales method on electrostatically actuated resonators. *J. Comput. Nonlinear Dyn.* 14 (4), 041006.
- Jauvtis, N., Williamson, C.H.K., 2003. Vortex-induced vibration of a cylinder with two degrees of freedom. *J. Fluids Struct.* 17 (7), 1035–1042.
- Jauvtis, N., Williamson, C.H.K., 2004. The effect of two degrees of freedom on vortex-induced vibration at low mass and damping. *J. Fluid Mech.* 509, 23–62.
- Jovanović, M.R., Schmid, P.J., Nichols, J.W., 2014. Sparsity-promoting dynamic mode decomposition. *Phys. Fluids* 26 (2), 024103.
- Keulegan, G.H., Carpenter, L.H., 1958. Forces on cylinders and plates in an oscillating fluid. *J. Res. Natl. Bur. Stand.* 2857, 423–440.
- Kválseth, T.O., 1985. Cautionary note about R^2 . *Am. Statist.* 39 (4), 279–285.

- Larsen, C.M., Vikestad, K., Yttervik, R., Passano, E., Baarholm, G.S., 2001. VIVANA Theory Manual. Marintek, Trondheim, Norway.
- Levin, D., 1998. The approximation power of moving least-squares. *Math. Comput.* 67 (224), 1517–1531.
- Li, S., Kaiser, E., Laima, S., Li, H., Brunton, S.L., Kutz, J.N., 2019. Discovering time-varying aerodynamics of a prototype bridge by sparse identification of nonlinear dynamical systems. *Phys. Rev. E* 100 (2), 022220.
- Lie, H., Kaasen, K.E., 2006. Modal analysis of measurements from a large-scale VIV model test of a riser in linearly sheared flow. *J. Fluids Struct.* 22 (4), 557–575.
- Liu, C., Fu, S., Zhang, M., Ren, H., 2017. Time varying hydrodynamics identification of a flexible riser under multi-frequency vortex-induced vibrations. In: ASME 2017 36th International Conference on Ocean, Offshore and Arctic Engineering. V002T08A029.
- Liu, C., Fu, S., Zhang, M., Ren, H., 2018. Time-varying hydrodynamics of a flexible riser under multi-frequency vortex-induced vibrations. *J. Fluids Struct.* 80, 217–244.
- Lu, Z., Fu, S., Zhang, M., Ren, H., 2019. An efficient time-domain prediction model for vortex-induced vibration of flexible risers under unsteady flows. *Mar. Struct.* 64, 492–519.
- Lu, Z., Fu, S., Zhang, M., Ren, H., Song, L., 2018. A modal space based direct method for vortex-induced vibration prediction of flexible risers. *Ocean Eng.* 152, 191–202.
- Maher, J., Finn, L., 2000. A combined time-frequency domain procedure to estimate riser fatigue caused by heave-induced vortex-induced vibration. In: Offshore Technology Conference.
- Marcoollo, H., Hinwood, J.B., 2006. On shear flow single mode lock-in with both cross-flow and in-line lock-in mechanisms. *J. Fluids Struct.* 22 (2), 197–211.
- Marzouk, O., Nayfeh, A.H., Akhtar, I., Arafat, H.N., 2007. Modeling steady-state and transient forces on a cylinder. *J. Vib. Control* 13 (7), 1065–1091.
- Nayfeh, A.H., Owis, F., Hajj, M.R., 2003. A model for the coupled lift and drag on a circular cylinder. In: ASME 2003 International Design Engineering Technical Conferences and Computers and Information in Engineering Conference. pp. 1289–1296.
- Paleologu, C., Benesty, J., Ciochino, S., 2008. A robust variable forgetting factor recursive least-squares algorithm for system identification. *IEEE Signal Process. Lett.* 15, 597–600.
- Pereira, F.R., Gonçalves, R.T., Pesce, C.P., Fujarra, A.L.C., Franzini, G.R., Mendes, P., 2013. A model scale experimental investigation on vortex-self induced vibrations (VSIV) of catenary risers. In: ASME 2013 32nd International Conference on Ocean, Offshore and Arctic Engineering. V007T08A029.
- Pesce, C.P., Franzini, G.R., Fujarra, A.L.C., Gonçalves, R.T., Salles, R., Mendes, P., 2017. Further experimental investigations on vortex self-induced vibrations (VSIV) with a small-scale catenary riser model. In: ASME 2017 36th International Conference on Ocean, Offshore and Arctic Engineering.
- Ren, T., Zhang, M., Fu, S., Song, L., 2018. Hydrodynamics of a flexible riser undergoing the vortex-induced vibration at high Reynolds number. *China Ocean Eng.* 32 (5), 570–581.
- Resvanis, T.L., 2014. Vortex-Induced Vibration of Flexible Cylinders in Time-Varying Flows (Ph.D. thesis). Massachusetts Institute of Technology.
- Resvanis, T.L., Vandiver, J.K., Fu, S., 2015. Ramp tests: A novel approach to VIV model testing of flexible cylinders using continuously varying towing speeds. In: ASME 2015 34th International Conference on Ocean, Offshore and Arctic Engineering. V002T08A059.
- Sarpkaya, T., 1986. Force on a circular cylinder in viscous oscillatory flow at low Keulegan–Carpenter numbers. *J. Fluid Mech.* 165, 61–71.
- Sarpkaya, T., 2010. Wave Forces on Offshore Structures. Cambridge university press.
- Schmid, P.J., 2010. Dynamic mode decomposition of numerical and experimental data. *J. Fluid Mech.* 656, 5–28.
- da Silveira, L.M.Y., Martins, C., Cunha, L.D., Pesce, C.P., 2009. An investigation on the effect of tension variation on VIV of risers. In: ASME 2007 26th International Conference on Offshore Mechanics and Arctic Engineering. pp. 267–275.
- Song, L., Fu, S., Cao, J., Ma, L., Wu, J., 2016a. An investigation into the hydrodynamics of a flexible riser undergoing vortex-induced vibration. *J. Fluids Struct.* 63, 325–350.
- Song, L., Fu, S., Ren, T., Lu, Z., 2017. Phase angles of the vibrations and hydrodynamic forces of the flexible risers undergoing vortex-induced vibration. *J. Offshore Mech. Arct. Eng.* 139 (3), 031803.
- Song, L., Fu, S., Zeng, Y., Chen, Y., 2016b. Hydrodynamic forces and coefficients on flexible risers undergoing vortex-induced vibrations in uniform flow. *J. Waterw. Port C.-ASCE* 142 (4), 04016001.
- Sumer, B.M., 2006. Hydrodynamics around Cylindrical Strucures, Vol. 26. World scientific.
- Swithenbank, S.B., 2007. Dynamics of Long Flexible Cylinders at High-Mode Number in Uniform and Sheared Flows (Ph.D. thesis). Massachusetts Institute of Technology.
- Swithenbank, S.B., Vandiver, J.K., 2007. Identifying the power-in region for vortex-induced vibrations of long flexible cylinders. In: ASME 2007 26th International Conference on Ocean, Offshore and Arctic Engineering. pp. 723–730.
- Tomás-Rodríguez, M., Banks, S.P., 2003. Linear approximations to nonlinear dynamical systems with applications to stability and spectral theory. *IMA J. Math. Control Inform.* 20 (1), 89–103.
- Tomás-Rodríguez, M., Banks, S.P., 2010. Linear, Time-Varying Approximations to Nonlinear Dynamical Systems: With Applications in Control and Optimization. Vol. 400. Springer Science & Business Media.
- Triantafyllou, M.S., 2003. VIVA Extended User's Manual. Department of Ocean Engineering, Massachusetts Institute of Technology.
- Vandiver, J.K., 1993. Dimensionless parameters important to the prediction of vortex-induced vibration of long, flexible cylinders in ocean currents. *J. Fluids Struct.* 7 (5), 423–455.
- Vandiver, J.K., Li, L., 2005. Shear7 V4. 4 Program Theoretical Manual. Department of Ocean Engineering, Massachusetts Institute of Technology.
- Vikestad, K., Vandiver, J.K., Larsen, C.M., 2000. Added mass and oscillation frequency for a circular cylinder subjected to vortex-induced vibrations and external disturbance. *J. Fluids Struct.* 14 (7), 1071–1088.
- Viotte, R., de Langre, E., Szydlowski, J., 2007. Computation of vortex-induced vibrations of long structures using a wake oscillator model: comparison with DNS and experiments. *Comput. Struct.* 85 (11–14), 1134–1141.
- Wang, J., Fu, S., Baarholm, R., 2018. Evaluation of vortex-induced vibration of a steel catenary riser in steady current and vessel motion-induced oscillatory current. *J. Fluids Struct.* 82, 412–431.
- Wang, J., Fu, S., Baarholm, R., Wu, J., Larsen, C.M., 2014. Fatigue damage of a steel catenary riser from vortex-induced vibration caused by vessel motions. *Mar. Struct.* 39, 131–156.
- Wang, J., Fu, S., Baarholm, R., Wu, J., Larsen, C.M., 2015a. Fatigue damage induced by vortex-induced vibrations in oscillatory flow. *Mar. Struct.* 40, 73–91.
- Wang, J., Fu, S., Baarholm, R., Wu, J., Larsen, C.M., 2015b. Out-of-plane vortex-induced vibration of a steel catenary riser caused by vessel motions. *Ocean Eng.* 109, 389–400.
- Wang, J., Fu, S., Wang, J., Li, H., Ong, M.C., 2017. Experimental investigation on vortex-induced vibration of a free-hanging riser under vessel motion and uniform current. *J. Offshore Mech. Arct. Eng.* 139 (4), 041703.

- Wang, J., Xiang, S., Fu, S., Cao, P., Yang, J., He, J., 2016. Experimental investigation on the dynamic responses of a free-hanging water intake riser under vessel motion. *Mar. Struct.* 50, 1–19.
- Willett, J.B., Singer, J.D., 1988. Another cautionary note about R^2 : Its use in weighted least-squares regression analysis. *Amer. Statist.* 42 (3), 236–238.
- Williamson, C.H.K., Govardhan, R., 2004. Vortex-induced vibrations. *Annu. Rev. Fluid Mech.* 36, 413–455.
- Wu, X., Ge, F., Hong, Y., 2012. A review of recent studies on vortex-induced vibrations of long slender cylinders. *J. Fluids Struct.* 28, 292–308.
- Wu, J., Lie, H., Larsen, C.M., Baarholm, R.J., 2015. An empirical heave induced VIV prediction model. In: ASME 2015 34th International Conference on Ocean, Offshore and Arctic Engineering.
- Wu, J., Lie, H., Larsen, C.M., Liapis, S., Baarholm, R., 2016. Vortex-induced vibration of a flexible cylinder: Interaction of the in-line and cross-flow responses. *J. Fluids Struct.* 63, 238–258.
- Zdravkovich, M.M., 1996. Different modes of vortex shedding: an overview. *J. Fluids Struct.* 10 (5), 427–437.
- Zhang, M., Fu, S., Song, L., Wu, J., Lie, H., Hu, H., 2018. Hydrodynamics of flexible pipe with staggered buoyancy elements undergoing vortex-induced vibrations. *J. Offshore Mech. Arct. Eng.* 140 (6), 061805.
- Zhang, H., Rowley, C.W., Deem, E.A., Cattafesta, L.N., 2019. Online dynamic mode decomposition for time-varying systems. *SIAM J. Appl. Dyn. Syst.* 18 (3), 1586–1609.